

Article

Static Response of 2D FG Porous Plates Resting on Elastic Foundation Using Midplane and Neutral Surfaces with Movable Constraints

Ammar Melaibari ¹, Salwa A. Mohamed ², Amr E. Assie ^{3,4}, Rabab A. Shanab ² and Mohamed A. Eltaher ^{1,*} 

¹ Mechanical Engineering Department, Faculty of Engineering, King Abdulaziz University, Jeddah P.O. Box 80204, Saudi Arabia

² Engineering Mathematics Department, Faculty of Engineering, Zagazig University, Zagazig P.O. Box 44519, Egypt

³ Mechanical Engineering Department, Faculty of Engineering, Jazan University, Jazan P.O. Box 45142, Saudi Arabia

⁴ Mechanical Design and Production Department, Faculty of Engineering, Zagazig University, Zagazig P.O. Box 44519, Egypt

* Correspondence: meltaher@kau.edu.sa or mohaeltaher@gmail.com; Tel.: +966-565518613 or +201001089561

Abstract: The current manuscript develops a novel mathematical formulation to portray the static deflection of a bi-directional functionally graded (BDFG) porous plate resting on an elastic foundation. The correctness of the static response produced by middle surface (MS) vs. neutral surface (NS) formulations, and the position of the boundary conditions, are derived in detail. The relation between in-plane displacement field variables on NS and on MS are derived. Bi-directional gradation through the thickness and axial direction are described by the power function; however, the porosity is depicted by cosine function. The displacement field of a plate is controlled by four variables higher order shear deformation theory to satisfy the zero shear at upper and lower surfaces. Elastic foundation is described by the Winkler–Pasternak model. The equilibrium equations are derived by Hamilton’s principles and then solved numerically by being discretized by the differential quadrature method (DQM). The proposed model is confirmed with former published analyses. The numerical parametric studies discuss the effects of porosity type, porosity coefficient, elastic foundations variables, axial and transverse gradation indices, formulation with respect to MS and NS, and position of boundary conditions (BCs) on the static deflection and stresses.

Keywords: static deflection of BDFG porous plates; middle and neutral surfaces; a four variables high shear deformation theory; movable and immovable BCs; numerical solution

MSC: 74G15



Citation: Melaibari, A.; Mohamed, S.A.; Assie, A.E.; Shanab, R.A.; Eltaher, M.A. Static Response of 2D FG Porous Plates Resting on Elastic Foundation Using Midplane and Neutral Surfaces with Movable Constraints. *Mathematics* **2022**, *10*, 4784. <https://doi.org/10.3390/math10244784>

Academic Editor: Efstratios Tzirtzilakis

Received: 27 November 2022

Accepted: 12 December 2022

Published: 15 December 2022

Publisher’s Note: MDPI stays neutral with regard to jurisdictional claims in published maps and institutional affiliations.



Copyright: © 2022 by the authors. Licensee MDPI, Basel, Switzerland. This article is an open access article distributed under the terms and conditions of the Creative Commons Attribution (CC BY) license (<https://creativecommons.org/licenses/by/4.0/>).

1. Introduction

Flexural structures such as beams, plates, shells are extensively used in numerous engineering applications such as in aerospace vehicles, naval, ships, constructions and so on. Through services, maintenances and repairs, these structures may be subjected to static, buckling, dynamic and impact loads, which will cause serious damage and failure [1], because of the excellent mechanical performances of the functionally graded material (FGM), which was invented in 1984 through the Japanese spaceplane project [2] and has a smooth change in compositions across the volume. Its use is being more widely investigated by scientists worldwide, where thousands of research papers on this material can be found in the open literature [3].

The gradation of materials in specific applications such as aerospace, nuclear, and shuttles needs two/three directional distributions of FGM rather than conventional 1D FGMs to overcome the stress concentration and thermal stresses, [4,5]. Nemat-Alla [6] suggested

two directional functionally graded materials that can endure super-high temperature and reduce thermal stresses. Lu et al. [7] developed semi-analytical 3D elasticity solutions by using a state space differential quadrature method in analyzing the mechanical response of orthotropic FG plates. In 2018, Bediz [8] studied a free vibration response of BDFGM curved parallelepipeds by using the numerical finite element method. Esmaeilzadeh et al. [9,10] used the dynamic relaxation method in exploring the dynamic response of stiffened BDFG porous plates exposed to a moving load. Ghatage et al. [11] developed a comprehensive literature survey on the modelling techniques and analysis of multi-directional FG structures such as beam, plate, and shell. Do et al. [12] used a non-uniform rational B-spline function to describe the variation of material distribution through three-dimensional spatial directions of FG plates and used it to evaluate the optimum gradation based on the natural frequency and buckling load as the objective function. Qin et al. [13–15] presented the effect of nonclassical boundary conditions on free vibrations of rotating functionally graded CNT-reinforced composite cylindrical shells. Karamanli et al. [16] utilized a finite element model to examine mechanical responses of multi-directional FG-strain gradient microplates.

During the fabrication process of FGMs, it is inevitable to create some porosities inside the material. The addition of porosities will result in different properties from the original FGM. Therefore, fully investigating the impact of porosity on the mechanical behaviors of FGM is essential [17,18]. Today, the mechanical responses of porous FG structures have attracted researchers and scientists, and most research has been conducted on static, vibration, and buckling problems of porous FG structures, [19,20]. Li et al. [21] studied the mechanical response of porous BDFG plates based on the first-order shear deformation theory and isogeometric analysis. Gao et al. [22] developed a mathematical model to study wave propagation in graphene platelets (GPLs)-reinforced FG metal foam plates integrated with piezoelectric actuator and sensor layers resting on an orthotropic visco-Pasternak medium in a magneto-electro-thermo environment. Based on the Navier series solution, Bekkaye et al. [23] examined analytically the bending and buckling of porous FG plates. Akbaş et al. [24,25] analyzed the dynamic response of thick FG porous sandwich beams resting on viscoelastic support by using the 2D plane stress finite element method. Ramteke et al. [26] investigated the nonlinear eigenfrequency characteristics of the doubly curved multi-directional FG porous panels by using the finite element technique. Ghandourah et al. [27] and Khadir et al. [28] studied the bending and buckling of FG-GRNC laminated plates via quasi-3d nonlocal strain gradient theory. Kabouche et al. [29] investigated the mechanical stability of BDFG porous sandwich plates by using a quasi-3D solution. Thi [30] analyzed numerically by finite element method the free vibration responses of porous FG plate with varying thickness resting on two-parameter elastic foundations in temperature conditions.

For elastic foundation analysis, Mohamed et al. [31] exploited the differential integral quadrature method to investigate nonlinear free and forced vibrations of buckled curved beams resting on nonlinear elastic foundations. Nguyen et al. [32] investigated the free vibration and static bending analysis of piezoelectric FGM plates resting on one area of the two-parameter elastic foundation. Phuc and Kim [33] examined free and forced vibration of piezoelectric FGM plates resting on two-parameter elastic foundations placed in thermal environments. Mohamed et al. [34] studied the snap-through instability of helicoidal composite curved beams surrounded by nonlinear elastic foundation by using Bernstein polynomials. Almitani et al. [35] and Mohamed et al. [36] developed exact solution of nonlinear behaviors of imperfect bioinspired helicoidal composite beams resting on elastic foundations. Hashemi et al. [37] studied nonlinear free vibration analysis of BDFG rectangular plate with porosities which are resting on Winkler–Pasternak elastic foundations. Van Vinh et al. [38] studied static bending and buckling analysis of BDFG porous plates resting on elastic foundations using an improved first-order shear deformation theory and FEM. Assie et al. [4] presented a mathematical model to investigate the static buckling of BDFG porous plates resting on elastic foundation based on unified shear theories.

Various studies were applied both to mid-surface and neutral surface formulations and their results compared; however, they come to conflicting conclusions. Larbi et al. [39] calculated the frequencies of movable simply supported beams based on the neutral plane and showed that the calculated frequencies were in very close agreement with the frequencies obtained from the mid-plane formulation. Eltaher et al. [40,41] studied FGM beams and showed that the vibration frequencies obtained from mid-plane and neutral plane formulations are different up to about 10%. Van Do et al. [42] proved that the deviation in thermal buckling for simply supported FG plate between neutral surface and mid-surface may reach 15%. Wang et al. [43] discussed the controversial conclusion in some research that the FGM beam must be based on the neutral plane formulation rather than the mid-plane one for correct solutions. They showed that, for FGM beams with clamped ends and movable simply supported ends, both formulations furnish the same frequency results. Fernando et al. [44] adopted a formulation based on a reference plane where the end supports are applied. The proposed formulation was used to calculate the vibration frequencies of laminated beams where the end immovable supports were placed at different heights.

The mentioned works indicate that there is no available study on the static deflection of BDFG porous plate resting on the elastic foundation based on middle surface (MS) and neutral surface (NS) formulations. Therefore, it will be presented in the current article. A four variables higher order shear deformation theory is developed to describe the kinematic field. Bi-directional gradations through the thickness and axial direction are described by the power function; however, the porosity is depicted by the cosine function. The equilibrium equations are derived by Hamilton’s principles and then solved numerically by being discretized by the differential quadrature method (DQM). The rest of the following article is organized as follows. Section 2 presents a mathematical formulation for the static porous BDFG plate resting on elastic foundation including constitutive equations, displacement field, gradation function, and porosity function relative to mid-surface and neutral surface. Numerical differential quadrature method (DQM) implementation and discretization for solving the partial differential equation are presented in Section 3. Problem validations are presented in Section 4 and numerical results and parametric studies are discussed in Section 5.

2. Theory and Formulation

2.1. A General Kinematic Field

Consider a rectangular plate of thickness h , length a in the x - direction and width b in the y - direction as shown in Figure 1. As known, the mid-plane is the plane at the mid-thickness and the neutral plane is the plane where the total axial internal force is equal to zero [41]. The displacement field based on a neutral physical surface and a four variables high shear deformation theory with no shear correction factors can be expressed as in [45–49].

$$u(x, y, z) = u_o(x, y) - (z - z_o) \frac{\partial w_b}{\partial x} - (F(z) - c_o) \frac{\partial w_s}{\partial x} \tag{1}$$

$$v(x, y, z) = v_o(x, y) - (z - z_o) \frac{\partial w_b}{\partial y} - (F(z) - c_o) \frac{\partial w_s}{\partial y} \tag{2}$$

$$w(x, y, z) = w_b(x, y) + w_s(x, y) \tag{3}$$

where:

- u_o, v_o, w_b and w_s are the displacements defined at the midplane.
- w_b and w_s stand for bending and shear parts, respectively
- z_o and c_o are variables defining the neutral surface and are evaluated by

$$z_o = \mu \frac{\int_{-h/2}^{h/2} z E(x, z, \phi_o) dz}{\int_{-h/2}^{h/2} E(x, z, \phi_o) dz}, \quad c_o = \mu \frac{\int_{-h/2}^{h/2} F(z) E(x, z, \phi_o) dz}{\int_{-h/2}^{h/2} E(x, z, \phi_o) dz} \tag{4}$$

where $E(x, z, \phi_0)$ is the equivalent Young’s modulus that will be identified by Equation (5).

- μ is defined as a factor equals one for neutral plane and zero for geometrical mid-plane.
- $F(z)$ is a shape function that estimates the distribution of transverse shear stress/strain (τ_{xz}, τ_{yz}) and may take several forms such as [50–54]:

$$F(z) = z - \left(\frac{h}{\pi}\right) \sin\left(\frac{\pi z}{h}\right) \tag{5}$$

$$F(z) = z\left(1 - e^{-2\left(\frac{z}{h}\right)^2}\right) \tag{6}$$

$$F(z) = \frac{4z^3}{3h^2} \tag{7}$$

$$F(z) = z\left(-\frac{1}{4} + \frac{5}{3} \frac{z^2}{h^2}\right) \tag{8}$$

$$F(z) = \frac{\frac{h}{\pi} \sinh\left(\frac{\pi z}{h}\right) - z}{\cos h\left(\frac{\pi}{2}\right) - 1} \tag{9}$$

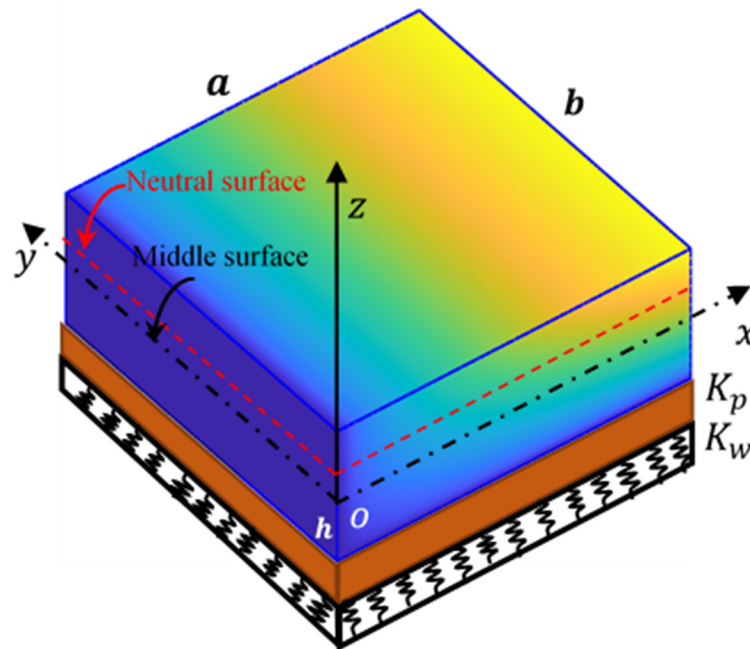


Figure 1. Schematic diagram of BDFG plate geometry with Winkler–Pasternak foundations.

The normal and shear strains associated with the displacement field in Equation (1) are expressed as follows [18,50]:

$$\epsilon_x = \bar{\epsilon}_x^0 - (z - z_0) \frac{\partial^2 w_b}{\partial x^2} - (F(z) - c_0) \frac{\partial^2 w_s}{\partial x^2} \tag{10}$$

$$\epsilon_y = \bar{\epsilon}_y^0 - (z - z_0) \frac{\partial^2 w_b}{\partial y^2} - (F(z) - c_0) \frac{\partial^2 w_s}{\partial y^2} \tag{11}$$

$$\gamma_{xy} = \bar{\gamma}_{xy}^0 - (z - z_0) \left(2 \frac{\partial^2 w_b}{\partial x \partial y}\right) - (F(z) - c_0) \left(2 \frac{\partial^2 w_s}{\partial x \partial y}\right) \tag{12}$$

$$\gamma_{yz} = G(z) \frac{\partial w_s}{\partial y} \tag{13}$$

$$\gamma_{xz} = G(z) \frac{\partial w_s}{\partial x} \tag{14}$$

in which

$$\bar{\epsilon}_x^o = \epsilon_x^o + z_{o,x} \frac{\partial w_b}{\partial x} + c_{o,x} \frac{\partial w_s}{\partial x}, \quad \epsilon_x^o = \frac{\partial u_0}{\partial x} \tag{15}$$

$$\bar{\epsilon}_y^o = \epsilon_y^o = \frac{\partial v_0}{\partial y} \tag{16}$$

$$\bar{\gamma}_{xy}^o = \gamma_{xy}^o + z_{o,x} \frac{\partial w_b}{\partial y} + c_{o,x} \frac{\partial w_s}{\partial y}, \quad \gamma_{xy}^o = \frac{\partial u_0}{\partial y} + \frac{\partial v_0}{\partial x} \tag{17}$$

$$F(z) = z - f(z), \quad G(z) = 1 - F'(z) = f'(z) \tag{18}$$

2.2. Constitutive Equations

The stress–strain relations for 2D shear deformation theory ($\epsilon_z = 0$), under isothermal conditions can be represented by:

$$\begin{bmatrix} \sigma_x \\ \sigma_y \\ \tau_{xy} \\ \tau_{yz} \\ \tau_{xz} \end{bmatrix} = \begin{bmatrix} Q_{11} & Q_{12} & 0 & 0 & 0 \\ Q_{12} & Q_{22} & 0 & 0 & 0 \\ 0 & 0 & Q_{66} & 0 & 0 \\ 0 & 0 & 0 & Q_{44} & 0 \\ 0 & 0 & 0 & 0 & Q_{55} \end{bmatrix} \begin{bmatrix} \epsilon_x \\ \epsilon_y \\ \gamma_{xy} \\ \gamma_{yz} \\ \gamma_{xz} \end{bmatrix} \tag{19}$$

where the plane stress stiffnesses for isotropic material are:

$$Q_{11} = Q_{22} = \frac{E}{1 - \nu^2}, \quad Q_{12} = \frac{\nu E}{1 - \nu^2} \tag{20}$$

$$Q_{44} = Q_{55} = Q_{66} = \frac{E}{2(1 + \nu)} \tag{21}$$

Assuming that the material properties are gradated through the thickness (z – axis) and axial (x – axis) according to the power law function including porosity as:

$$P(x, z, \phi_o) = [P_m + P_{cm} \left(\frac{1}{2} + \frac{z}{h}\right)^{n_z} \left(\frac{x}{a}\right)^{n_x}] [1 - \Phi(z)] \tag{22}$$

$$P_{cm} = P_c - P_m \tag{23}$$

in which P denotes a generic material property like Young’s modulus (E), and density (ρ) through z – and x – directions according to power laws with indices, n_z and n_x , respectively, [15,18,55]. Subscripts c and m donate the ceramic and metal phases. h and a are the thickness of plate and length in x -direction, respectively. $\Phi(z)$ is a porosity distribution function having the following three different types [56–58]:

$$\text{Type 1 (center enhanced) : } \Phi(z) = \phi_o \cos\left(\frac{\pi}{h}z\right) \tag{24}$$

$$\text{Type 2 (top enhanced) : } \Phi(z) = \phi_o \cos\left(\frac{\pi}{2}\left(\frac{z}{h} + \frac{1}{2}\right)\right) \tag{25}$$

$$\text{Type 3 (bottom enhanced) : } \Phi(z) = \phi_o \cos\left(\frac{\pi}{2}\left(\frac{z}{h} - \frac{1}{2}\right)\right) \tag{26}$$

where ϕ_o is the porosity coefficient.

2.3. Hamilton’s Principles and Governing Equations

The governing equations of equilibrium and associated boundary conditions of the developed model are derived using Hamilton’s Principles, which can be described as

$$\int_0^T \delta(U + V + U_{ef}) dt = 0 \tag{27}$$

where the virtual potential work of applied loads can be expressed in the form δV :

$$\delta V = - \int_A q \delta(w_b + w_s) dA \tag{28}$$

and the variation of potential energy of the elastic foundation (Winkler–Pasternak type) can be expressed as:

$$\delta U_{ef} = \int_A [K_w(w_b + w_s) - K_p \nabla^2(w_b + w_s)] \delta(w_b + w_s) dA \tag{29}$$

$$\text{where : } \nabla^2(w_b + w_s) = \frac{\partial^2(w_b + w_s)}{\partial x^2} + \frac{\partial^2(w_b + w_s)}{\partial y^2}$$

The virtual strain energy δU can be evaluated by

$$\delta U = \int_V (\sigma_x \delta \epsilon_x + \sigma_y \delta \epsilon_y + \tau_{xy} \delta \gamma_{xy} + \tau_{xz} \delta \gamma_{xz} + \tau_{yz} \delta \gamma_{yz}) dV \tag{30}$$

The virtual strain energy δU in terms of stress resultants is derived as: -

$$\begin{aligned} \delta U = \int_A \left[N_x \delta \epsilon_x^0 + N_y \delta \epsilon_y^0 + N_{xy} \delta \gamma_{xy}^0 - M_x^b \frac{\partial^2 \delta w_b}{\partial x^2} - M_y^b \frac{\partial^2 \delta w_b}{\partial y^2} \right. \\ \left. - M_{xy}^b \left(2 \frac{\partial^2 \delta w_b}{\partial x \partial y} \right) - M_x^s \frac{\partial^2 \delta w_s}{\partial x^2} - M_y^s \frac{\partial^2 \delta w_s}{\partial y^2} - M_{xy}^s \left(2 \frac{\partial^2 \delta w_s}{\partial x \partial y} \right) \right. \\ \left. + S_{yz}^s \frac{\partial \delta w_s}{\partial y} + S_{xz}^s \frac{\partial \delta w_s}{\partial x} \right] dA \tag{31} \end{aligned}$$

Substituting Equations (28)–(31) for δV , δU_{ef} and δU , respectively, into Equation (27) and performing integration by parts, the equations of the FGM porous plate in terms of stress resultants are obtained as:

$$\delta u_o : \frac{\partial N_x}{\partial x} + \frac{\partial N_{xy}}{\partial y} = 0 \tag{32}$$

$$\delta v_o : \frac{\partial N_{xy}}{\partial x} + \frac{\partial N_y}{\partial y} = 0 \tag{33}$$

$$\delta w_b : \frac{\partial^2 M_x^b}{\partial x^2} + 2 \frac{\partial^2 M_{xy}^b}{\partial x \partial y} + \frac{\partial^2 M_y^b}{\partial y^2} + q + K_p \nabla^2(w_b + w_s) - K_w(w_b + w_s) = 0 \tag{34}$$

$$\delta w_s : \frac{\partial^2 M_x^s}{\partial x^2} + 2 \frac{\partial^2 M_{xy}^s}{\partial x \partial y} + \frac{\partial^2 M_y^s}{\partial y^2} + \frac{\partial S_{yz}^s}{\partial y} + \frac{\partial S_{xz}^s}{\partial x} + q + K_p \nabla^2(w_b + w_s) - K_w(w_b + w_s) = 0 \tag{35}$$

Associated with the following boundary conditions:

$$\delta v_o : (N_{xy} \bar{n}_x + N_y \bar{n}_y) \delta v_o = 0 \tag{36}$$

$$\delta v_o : (N_{xy} \bar{n}_x + N_y \bar{n}_y) \delta v_o = 0 \tag{37}$$

$$\delta w_b : \left((M_{x,x}^b + M_{xy,y}^b) \bar{n}_x + (M_{xy,x}^b + M_{y,y}^b) \bar{n}_y \right) \delta w_b = 0 \tag{38}$$

$$\frac{\partial \delta w_b}{\partial x} : (M_x^b \bar{n}_x + M_{xy}^b \bar{n}_y) \frac{\partial \delta w_b}{\partial x} = 0 \tag{39}$$

$$\frac{\partial \delta w_b}{\partial y} : (M_{xy}^b \bar{n}_x + M_y^b \bar{n}_y) \frac{\partial \delta w_b}{\partial y} = 0 \tag{40}$$

$$\delta w_s : \left((M_{x,x}^s + M_{xy,y}^s + S_{xz}^s) \bar{n}_x + (M_{xy,x}^s + M_{y,y}^s + S_{yz}^s) \bar{n}_y \right) \delta w_s = 0 \tag{41}$$

$$\frac{\partial \delta w_s}{\partial x} : (M_x^s \bar{n}_x + M_{xy}^s \bar{n}_y) \frac{\partial \delta w_s}{\partial x} = 0 \tag{42}$$

$$\frac{\partial \delta w_s}{\partial y} : (M_{xy}^s \bar{n}_x + M_y^s \bar{n}_y) \frac{\partial \delta w_s}{\partial y} = 0 \tag{43}$$

where \bar{n}_x and \bar{n}_y are the components of the outward normal at boundaries.

The stress resultants can be expressed in terms of generalized displacement (u_o, v_o, w_b, w_s) in a matrix form as:

$$\begin{bmatrix} N_x \\ N_y \\ N_{xy} \\ M_x^b \\ M_y^b \\ M_{xy}^b \\ M_x^s \\ M_y^s \\ M_{xy}^s \end{bmatrix} = \begin{bmatrix} A_{11} & A_{12} & 0 & B_{11} & B_{12} & 0 & B_{11}^s & B_{12}^s & 0 \\ A_{12} & A_{22} & 0 & B_{12} & B_{22} & 0 & B_{12}^s & B_{22}^s & 0 \\ 0 & 0 & A_{66} & 0 & 0 & B_{66} & 0 & 0 & B_{66}^s \\ B_{11} & B_{12} & 0 & D_{11} & D_{12} & 0 & D_{11}^s & D_{12}^s & 0 \\ B_{12} & B_{22} & 0 & D_{12} & D_{22} & 0 & D_{12}^s & D_{22}^s & 0 \\ 0 & 0 & B_{66} & 0 & 0 & D_{66} & 0 & 0 & D_{66}^s \\ B_{11}^s & B_{12}^s & 0 & D_{11}^s & D_{12}^s & 0 & H_{11}^s & H_{12}^s & 0 \\ B_{12}^s & B_{22}^s & 0 & D_{12}^s & D_{22}^s & 0 & H_{12}^s & H_{22}^s & 0 \\ 0 & 0 & B_{66}^s & 0 & 0 & D_{66}^s & 0 & 0 & H_{66}^s \end{bmatrix} \begin{bmatrix} \bar{\epsilon}_x^0 \\ \bar{\epsilon}_y^0 \\ \bar{\gamma}_{xy}^0 \\ -\partial^2 w_b / \partial^2 x \\ -\partial^2 w_b / \partial^2 y \\ -2\partial^2 w_b / \partial x \partial y \\ -\partial^2 w_s / \partial^2 x \\ -\partial^2 w_s / \partial^2 y \\ -2\partial^2 w_s / \partial x \partial y \end{bmatrix} \tag{44}$$

$$\begin{bmatrix} S_{yz}^s \\ S_{xz}^s \end{bmatrix} = \begin{bmatrix} A_{44}^s & 0 \\ 0 & A_{55}^s \end{bmatrix} \begin{bmatrix} \partial w_s / \partial y \\ \partial w_s / \partial x \end{bmatrix} \tag{45}$$

By substituting Equations (5)–(9), (10)–(18), (44) and (45) into Equations (32)–(35), the above governing equations can be acquired in terms of displacements as the following:

$$\begin{aligned} \delta u_o : & A_{11}(x) \left(\frac{\partial^2 u_o}{\partial x^2} + z_{o,xx} \frac{\partial w_b}{\partial x} + z_{o,x} \frac{\partial^2 w_b}{\partial x^2} + c_{o,xx} \frac{\partial w_s}{\partial x} + c_{o,x} \frac{\partial^2 w_s}{\partial x^2} \right) + (A_{12}(x) + \\ & A_{66}(x)) \frac{\partial^2 v_o}{\partial x \partial y} + A_{66}(x) \left(\frac{\partial^2 u_o}{\partial y^2} + z_{o,x} \frac{\partial^2 w_b}{\partial y^2} + c_{o,x} \frac{\partial^2 w_s}{\partial y^2} \right) + A_{11,x}(x) \bar{\epsilon}_x^0 + A_{12,x}(x) \bar{\epsilon}_y^0 - \\ & (B_{12}(x) + 2B_{66}(x)) \frac{\partial^3 w_b}{\partial x \partial y^2} - (B_{12}^s(x) + 2B_{66}^s(x)) \frac{\partial^3 w_s}{\partial x \partial y^2} - B_{11}(x) \frac{\partial^3 w_b}{\partial x^3} - B_{11}^s(x) \frac{\partial^3 w_s}{\partial x^3} - \\ & B_{11,x}(x) \frac{\partial^2 w_b}{\partial x^2} - B_{12,x}(x) \frac{\partial^2 w_b}{\partial y^2} - B_{11,x}^s(x) \frac{\partial^2 w_s}{\partial x^2} - B_{12,x}^s(x) \frac{\partial^2 w_s}{\partial y^2} = 0 \end{aligned} \tag{46}$$

$$\begin{aligned} \delta v_o : & (A_{12}(x) + A_{66}(x)) \left(\frac{\partial^2 u_o}{\partial x \partial y} + z_{o,x} \frac{\partial^2 w_b}{\partial x \partial y} + c_{o,x} \frac{\partial^2 w_s}{\partial x \partial y} \right) + A_{22}(x) \frac{\partial^2 v_o}{\partial y^2} \\ & + A_{66}(x) \left(\frac{\partial^2 v_o}{\partial x^2} + z_{o,xx} \frac{\partial w_b}{\partial y} + c_{o,xx} \frac{\partial w_s}{\partial y} \right) + A_{66,x}(x) \bar{\gamma}_{xy}^0 \\ & - (B_{12}(x) + 2B_{66}(x)) \frac{\partial^3 w_b}{\partial x^2 \partial y} - (B_{12}^s(x) + 2B_{66}^s(x)) \frac{\partial^3 w_s}{\partial x^2 \partial y} \\ & - B_{22}(x) \frac{\partial^3 w_b}{\partial y^3} - B_{22}^s(x) \frac{\partial^3 w_s}{\partial y^3} - 2B_{66,x}(x) \frac{\partial^2 w_b}{\partial x \partial y} - 2B_{66,x}^s(x) \frac{\partial^2 w_s}{\partial x \partial y} \end{aligned} \tag{47}$$

$$\begin{aligned} \delta w_b : & B_{11}(x) \left(\frac{\partial^3 u_o}{\partial x^3} + z_{o,xxx} \frac{\partial w_b}{\partial x} + 2z_{o,xx} \frac{\partial^2 w_b}{\partial x^2} + z_{o,x} \frac{\partial^3 w_b}{\partial x^3} + c_{o,xxx} \frac{\partial w_s}{\partial x} + \right. \\ & 2c_{o,xx} \frac{\partial^2 w_s}{\partial x^2} + c_{o,x} \frac{\partial^3 w_s}{\partial x^3} \left. \right) + B_{22}(x) \frac{\partial^3 v_o}{\partial y^3} + (B_{12}(x) + 2B_{66}(x)) \left(\frac{\partial^3 u_o}{\partial x \partial y^2} + \right. \\ & \left. \frac{\partial^3 v_o}{\partial x^2 \partial y} + z_{o,x} \frac{\partial^3 w_b}{\partial x \partial y^2} + c_{o,x} \frac{\partial^3 w_s}{\partial x \partial y^2} \right) + 2B_{66}(x) \left(z_{o,xx} \frac{\partial^2 w_b}{\partial y^2} + c_{o,xx} \frac{\partial^2 w_s}{\partial y^2} \right) + 2(B_{12,x}(x) + \\ & B_{66,x}(x)) \frac{\partial^2 v_o}{\partial x \partial y} + 2B_{66,x}(x) \left(\frac{\partial^2 u_o}{\partial y^2} + z_{o,x} \frac{\partial^2 w_b}{\partial y^2} + c_{o,x} \frac{\partial^2 w_s}{\partial y^2} \right) + 2B_{11,x}(x) \left(\frac{\partial^2 u_o}{\partial x^2} + z_{o,xx} \frac{\partial w_b}{\partial x} + \right. \\ & \left. z_{o,x} \frac{\partial^2 w_b}{\partial x^2} + c_{o,xx} \frac{\partial w_s}{\partial x} + c_{o,x} \frac{\partial^2 w_s}{\partial x^2} \right) + B_{11,xx}(x) \bar{\epsilon}_x^0 + B_{12,xx}(x) \bar{\epsilon}_y^0 - D_{11}(x) \frac{\partial^4 w_b}{\partial x^4} - \\ & D_{22}(x) \frac{\partial^4 w_b}{\partial y^4} - 2(D_{12}(x) + 2D_{66}(x)) \frac{\partial^4 w_b}{\partial x^2 \partial y^2} - D_{11}^s(x) \frac{\partial^4 w_s}{\partial x^4} - D_{22}^s(x) \frac{\partial^4 w_s}{\partial y^4} - \\ & 2(D_{12}^s(x) + 2D_{66}^s(x)) \frac{\partial^4 w_s}{\partial x^2 \partial y^2} - 2D_{11,x}(x) \frac{\partial^3 w_b}{\partial x^3} - 2(D_{12,x}(x) + 2D_{66,x}(x)) \frac{\partial^3 w_b}{\partial x \partial y^2} - \\ & 2D_{11,x}^s(x) \frac{\partial^3 w_s}{\partial x^3} - 2(D_{12,x}(x) + 2D_{66,x}(x)) \frac{\partial^3 w_b}{\partial x \partial y^2} - D_{11,xx}(x) \frac{\partial^2 w_b}{\partial x^2} - D_{12,xx}(x) \frac{\partial y}{\partial x} - \\ & D_{11,xx}^s(x) \frac{\partial^2 w_s}{\partial x^2} - D_{12,xx}^s(x) \frac{\partial^2 w_s}{\partial y^2} + q + K_p \nabla^2 (w_b + w_s) - K_w (w_b + w_s) = 0 \end{aligned} \tag{48}$$

$$\begin{aligned}
 \delta w_s : & B_{11}^s(x) \left(\frac{\partial^3 u_o}{\partial x^3} + z_{o,xx} \frac{\partial w_b}{\partial x} + 2z_{o,xx} \frac{\partial^2 w_b}{\partial x^2} + z_{o,x} \frac{\partial^3 w_b}{\partial x^3} + c_{o,xxx} \frac{\partial w_s}{\partial x} + \right. \\
 & 2c_{o,xx} \frac{\partial^2 w_s}{\partial x^2} + c_{o,x} \frac{\partial^3 w_s}{\partial x^3} \left. \right) + B_{22}^s(x) \frac{\partial^3 v_o}{\partial y^3} + (B_{12}^s(x) + 2B_{66}^s(x)) \left(\frac{\partial^3 u_o}{\partial x \partial y^2} + \right. \\
 & \left. \frac{\partial^3 v_o}{\partial x^2 \partial y} + z_{o,x} \frac{\partial^3 w_b}{\partial x \partial y^2} + c_{o,x} \frac{\partial^3 w_s}{\partial x \partial y^2} \right) + 2B_{66}^s(x) \left(z_{o,xx} \frac{\partial^2 w_b}{\partial y^2} + c_{o,xx} \frac{\partial^2 w_s}{\partial y^2} \right) + 2 \left(B_{12,x}^s(x) + \right. \\
 & \left. B_{66,x}^s(x) \right) \frac{\partial^2 v_o}{\partial x \partial y} + 2B_{66,x}^s(x) \left(\frac{\partial^2 u_o}{\partial y^2} + z_{o,x} \frac{\partial^2 w_b}{\partial y^2} + c_{o,x} \frac{\partial^2 w_s}{\partial y^2} \right) + 2B_{11,x}^s(x) \left(\frac{\partial^2 u_o}{\partial x^2} + z_{o,xx} \frac{\partial w_b}{\partial x} + \right. \\
 & \left. z_{o,x} \frac{\partial^2 w_b}{\partial x^2} + c_{o,xx} \frac{\partial w_s}{\partial x} + c_{o,x} \frac{\partial^2 w_s}{\partial x^2} \right) + B_{11,xx}^s(x) \bar{\epsilon}_x^0 + B_{12,xx}^s(x) \bar{\epsilon}_y^0 - \\
 D_{11}^s(x) \frac{\partial^4 w_b}{\partial x^4} - D_{22}^s(x) \frac{\partial^4 w_b}{\partial y^4} - 2(D_{12}^s(x) + 2D_{66}^s(x)) \frac{\partial^4 w_b}{\partial x^2 \partial y^2} - H_{11}^s(x) \frac{\partial^4 w_s}{\partial x^4} - H_{22}^s(x) \frac{\partial^4 w_s}{\partial y^4} - \\
 & 2(H_{12}^s(x) + 2H_{66}^s(x)) \frac{\partial^4 w_s}{\partial x^2 \partial y^2} - 2D_{11,x}^s(x) \frac{\partial^3 w_b}{\partial x^3} - 2(D_{12,x}^s(x) + 2D_{66,x}^s(x)) \frac{\partial^3 w_b}{\partial x \partial y^2} - \\
 & 2H_{11,x}^s(x) \frac{\partial^3 w_s}{\partial x^3} - 2(H_{12,x}^s(x) + 2H_{66,x}^s(x)) \frac{\partial^3 w_s}{\partial x \partial y^2} - D_{11,xx}^s(x) \frac{\partial^2 w_b}{\partial x^2} - D_{12,xx}^s(x) \frac{\partial^2 w_b}{\partial y^2} - \\
 & \left(H_{11,xx}^s(x) - A_{55}^s(x) \right) \frac{\partial^2 w_s}{\partial x^2} - \left(H_{12,xx}^s(x) - A_{44}^s(x) \right) \frac{\partial^2 w_s}{\partial y^2} + A_{55,x}^s(x) \frac{\partial w_s}{\partial x} + q + \\
 & K_P \nabla^2 (w_b + w_s) - K_w (w_b + w_s) = 0
 \end{aligned} \tag{49}$$

Note that: The subscripts $_x$, $_{,xx}$, and $_{,xxx}$ denote first, second, and third derivative with respect to x , respectively.

2.4. Equivalent Stiffnesses Based on Geometrical Midplane (MS)

To consider the geometric middle surface of the plate, put z_o and c_o as zero-valued ($\mu = 0$) in displacement and strain fields of Equations (1)–(18); where rigidities terms are obtained as functions of x as:

$$\left[(A_{ij}(x), B_{ij}(x), D_{ij}(x), B_{ij}^s(x), D_{ij}^s(x), H_{ij}^s(x)) \right] = \int_{-h/2}^{h/2} Q_{ij}(x, z, \phi_o) \left[1, z, z^2, F(z), zF(z), (F(z))^2 \right] dz, \quad ij = 11, 12, 22, 66 \tag{50}$$

$$A_{ij}^s(x) = \int_{-h/2}^{h/2} Q_{ij}(x, z, \phi_o) (G(z))^2 dz, \quad ij = 44, 55 \tag{51}$$

$Q_{ij}(x, z, \phi_o)$ and $E(x, z, \phi_o)$ are defined by Equations (19) and (22), respectively.

2.5. Equivalent Stiffnesses Based on Neutral Physical Surface (NS)

Due to the use of z_o and c_o ($\mu = 1$) defined by Equation (4) in the displacement field of Equation (1), the plate stiffnesses $B_{ij}(x)$ and $B_{ij}^s(x)$ are zero-valued. Subsequently, stretching–bending couplings in Equation (44) die out. Therefore, rigidity terms are modified as functions of x to:

$$(A_{ij}(x), D_{ij}(x), D_{ij}^s(x), H_{ij}^s(x)) = \int_{-h/2}^{h/2} Q_{ij}(x, z, \phi_o) (1, (z - z_o)^2, (z - z_o)(F(z) - c_o), (F(z) - c_o)^2) dz, \quad ij = 11, 12, 22, 66 \tag{52}$$

$$A_{ij}^s(x) = \int_{-h/2}^{h/2} Q_{ij}(x, z, \phi_o) (G(z))^2 dz, \quad ij = 44, 55 \tag{53}$$

The equations of motion based on the physical neutral surface can be obtained by modifying Equations (32)–(35) and (46)–(49) utilizing rigidity terms defined by Equations (52) and (53) instead of those employing the geometric midplane. It is worth noting that stretching–bending couplings vanish in these adjusted equations because of the disappearance of the stiffnesses $B_{ij}(x)$ and $B_{ij}^s(x)$.

3. Numerical Technique

The differential quadrature method (DQM) is a powerful discretization method for the numerical solution of partial differential equations (PDE) appearing in engineering [59]. As compared to the conventional finite element and finite difference methods, DQM can obtain very accurate numerical results using a considerably smaller number of grid points and hence, requiring relatively little computational cost. Another advantage of DQM is that discretization of boundary conditions, even those involving higher order derivatives,

is easy and accurate (Shu [59], Shanab et al. [60]). These advantages make this method preferable especially for problems with sufficiently smooth solutions such as the ones considered in the present study.

A set of four partial differential governing equations and associated boundary conditions were developed based on stress resultants to model the static response of BDFG plates in Equations (11) and (12), respectively. The assumption that the material properties change in the x - direction complicates the governing equations since they become variable coefficients and consequently, no analytical solution can be found. In addition, derivatives of z_0 and c_0 with respect to x are to be neglected. In this work, the Differential/Integral Quadrature Method (DIQM) [61,62] is developed to numerically solve the governing equations of a rectangular plate ($0 \leq x \leq a, 0 \leq y \leq b$) with the following boundary conditions:

Clamped BCs:

$$u_0 = v_0 = w_b = w_s = \frac{\partial w_b}{\partial x} = \frac{\partial w_s}{\partial x} = 0 \text{ at } x = 0, x = a \tag{54}$$

$$u_0 = v_0 = w_b = w_s = \frac{\partial w_b}{\partial y} = \frac{\partial w_s}{\partial y} = 0 \text{ at } y = 0, y = b \tag{55}$$

Simply supported BCs

Type 1 (S_m) (movable normal in-plane displacement)

$$N_x = v_0 = w_b = w_s = M_x^b = M_x^s = 0 \text{ at } x = 0, x = a \tag{56}$$

$$u_0 = N_y = w_b = w_s = M_y^b = M_y^s = 0 \text{ at } y = 0, y = b \tag{57}$$

Type 2 (S_{im}) (immovable normal in-plane displacement)

$$u_0 = v_0 = w_b = w_s = M_x^b = M_x^s = 0 \text{ at } x = 0, x = a \tag{58}$$

$$u_0 = v_0 = w_b = w_s = M_y^b = M_y^s = 0 \text{ at } y = 0, y = b \tag{59}$$

If NS formulation is considered, i.e., $z_0 \neq 0, c_0 \neq 0$, the appreciations S_{im-NS} and S_{m-NS} are used. If MS formulation is considered, i.e., $z_0 = c_0 = 0$, the appreciations S_{im-MS} and S_{m-MS} are used. For CCCC, it is C_{NS} (immovable with NS formulation) and C_{MS} (immovable with MS formulation).

3.1. DQM Implementation for PDE

The DIQM was employed by [62] to solve linear and nonlinear integro-differential equations. It was found that DIQM provides highly accurate results using only a few grid points. It transforms the integro-differential equations into a system of algebraic equations. In this section, the details of DIQM for partial differential equations are presented. Consider a partial differential equation in the unknown function $u(x, y)$. The 2D domain of the independent variables $0 < x < a, 0 < y < b$ is discretized by n and m points, respectively. The unknowns $u_{ij} = u(x_j, y_i), i = 1, \dots, m, j = 1, \dots, n$ defined on the rectangular domain are rearranged vector after vector to form the whole unknown vector

$$U = [u_{11}, u_{21}, \dots, u_{m1}, u_{12}, u_{22}, \dots, u_{m2}, \dots, \dots, u_{1n}, u_{2n}, \dots, u_{mn}]^T \tag{60}$$

Using classical definitions for DQM in one dimension [59], let D_x be the first order derivative matrix with respect to x of dimension $n \times n$ and let D_y be the first order derivative matrix with respect to y of dimension $m \times m$. To be consistent with the arrangement of unknowns given in Equation (60) for vector U , the Kronecker product is used to construct global derivative matrices of dimension $(mn \times mn)$ as

$$\begin{aligned} \mathbb{D}_x &= \text{Kronecker}(D_x, I(m)) \\ \mathbb{D}_y &= \text{Kronecker}(I(n), D_y) \end{aligned} \tag{61}$$

where $I(n)$ and $I(m)$ are the identity matrices of dimensions $(n \times n)$ and $(m \times m)$, respectively. Based on Equation (61), DQM can approximate higher and mixed partial derivatives such as $\partial^2 u / \partial x^2$, $\partial^2 u / \partial y^2$, $\partial^2 u / \partial x \partial y$ by $\mathbb{D}_{xx} U$, $\mathbb{D}_{yy} U$ and $\mathbb{D}_{xy} U$, respectively, where $\mathbb{D}_{xx} = \mathbb{D}_x^2$, $\mathbb{D}_{yy} = \mathbb{D}_y^2$, and $\mathbb{D}_{xy} = \mathbb{D}_x \mathbb{D}_y$.

3.2. DQM Discretization for PDF

The governing equations for the BDFG plate consist of four variable-coefficient partial differential equations in the unknowns $u_0(x, y)$, $v_0(x, y)$, $w_b(x, y)$, and $w_s(x, y)$. They are discretized by DQM as the unknown vectors U, V, W_b and W_s each of dimension $(nm \times 1)$. Moreover, the variable coefficients $A_{ij}(x), B_{ij}(x), D_{ij}(x), B_{ij}^s(x), D_{ij}^s(x), H_{ij}^s(x)$, $ij = 11, 12, 22, 66$, and $A_{ij}^s(x)$, $ij = 44, 55$ are defined for MS and NS formulations in Equations (50)–(53), respectively. These coefficients are computed by IQM and arranged as $(nm \times 1)$ vectors $\mathcal{A}_{ij}, \mathcal{B}_{ij}, \mathcal{D}_{ij}, \mathcal{B}_{ij}^s, \mathcal{D}_{ij}^s, \mathcal{H}_{ij}^s$, $ij = 11, 12, 22, 66$, and $\mathcal{A}_{44}^s, \mathcal{A}_{55}^s$. For the convenience of applying DQM to discretize the variable-coefficient partial differential equations, a special matrices multiplication operator is introduced. The operator ‘ \circ ’ is defined such that for a vector \mathcal{V} of dimensions $(n \times 1)$ and a matrix \mathcal{M} of dimensions $(n \times m)$ (i.e., each of \mathcal{V} and \mathcal{M} must have the same number of rows), $\mathcal{V} \circ \mathcal{M} = \mathcal{Y}$, implies that \mathcal{Y} is a $(n \times m)$ matrix such that $\mathcal{Y}_{ij} = \mathcal{V}_i \mathcal{M}_{ij}$.

Applying the DIQM as described in Section 3.1, the stress resultants can be written as

$$\begin{bmatrix} N_x \\ N_y \\ N_{xy} \\ M_x^b \\ M_y^b \\ M_{xy}^b \\ M_x^s \\ M_y^s \\ M_{xy}^s \end{bmatrix} = \begin{bmatrix} \mathcal{K}_{N_x} \\ \mathcal{K}_{N_y} \\ \mathcal{K}_{N_{xy}} \\ \mathcal{K}_{M_x^b} \\ \mathcal{K}_{M_y^b} \\ \mathcal{K}_{M_{xy}^b} \\ \mathcal{K}_{M_x^s} \\ \mathcal{K}_{M_y^s} \\ \mathcal{K}_{M_{xy}^s} \end{bmatrix} \mathcal{X} \tag{62}$$

where each of $\{\mathcal{K}_{N_x}, \mathcal{K}_{N_y}, \dots, \mathcal{K}_{M_{xy}^s}\}$ is $(nm \times 4nm)$ matrix,

$$\mathcal{X} = [U^T, V^T, W_b^T, W_s^T]^T, \tag{63}$$

$$\begin{bmatrix} \mathcal{K}_{N_x} \\ \mathcal{K}_{N_y} \\ \mathcal{K}_{N_{xy}} \\ \mathcal{K}_{M_x^b} \\ \mathcal{K}_{M_y^b} \\ \mathcal{K}_{M_{xy}^b} \\ \mathcal{K}_{M_x^s} \\ \mathcal{K}_{M_y^s} \\ \mathcal{K}_{M_{xy}^s} \end{bmatrix} =$$

$$\begin{bmatrix} \mathcal{A}_{11} \circ \mathbb{D}_x & \mathcal{A}_{12} \circ \mathbb{D}_y & -(\mathcal{B}_{11} \circ \mathbb{D}_{xx} + \mathcal{B}_{12} \circ \mathbb{D}_{yy}) & -(\mathcal{B}_{11}^s \circ \mathbb{D}_{xx} + \mathcal{B}_{12}^s \circ \mathbb{D}_{yy}) \\ \mathcal{A}_{12} \circ \mathbb{D}_x & \mathcal{A}_{22} \circ \mathbb{D}_y & -(\mathcal{B}_{12} \circ \mathbb{D}_{xx} + \mathcal{B}_{22} \circ \mathbb{D}_{yy}) & -(\mathcal{B}_{12}^s \circ \mathbb{D}_{xx} + \mathcal{B}_{22}^s \circ \mathbb{D}_{yy}) \\ \mathcal{A}_{66} \circ \mathbb{D}_y & \mathcal{A}_{66} \circ \mathbb{D}_x & -2\mathcal{B}_{66} \circ \mathbb{D}_{xy} & -2\mathcal{B}_{66}^s \circ \mathbb{D}_{xy} \\ \mathcal{B}_{11} \circ \mathbb{D}_x & \mathcal{B}_{12} \circ \mathbb{D}_y & -(\mathcal{D}_{11} \circ \mathbb{D}_{xx} + \mathcal{D}_{12} \circ \mathbb{D}_{yy}) & -(\mathcal{D}_{11}^s \circ \mathbb{D}_{xx} + \mathcal{D}_{12}^s \circ \mathbb{D}_{yy}) \\ \mathcal{B}_{12} \circ \mathbb{D}_x & \mathcal{B}_{22} \circ \mathbb{D}_y & -(\mathcal{D}_{12} \circ \mathbb{D}_{xx} + \mathcal{D}_{22} \circ \mathbb{D}_{yy}) & -(\mathcal{D}_{12}^s \circ \mathbb{D}_{xx} + \mathcal{D}_{22}^s \circ \mathbb{D}_{yy}) \\ \mathcal{B}_{66} \circ \mathbb{D}_y & \mathcal{B}_{66} \circ \mathbb{D}_x & -2\mathcal{D}_{66} \circ \mathbb{D}_{xy} & -2\mathcal{D}_{66}^s \circ \mathbb{D}_{xy} \\ \mathcal{B}_{11}^s \circ \mathbb{D}_x & \mathcal{B}_{12}^s \circ \mathbb{D}_y & -(\mathcal{D}_{11} \circ \mathbb{D}_{xx} + \mathcal{D}_{12} \circ \mathbb{D}_{yy}) & -(\mathcal{H}_{11}^s \circ \mathbb{D}_{xx} + \mathcal{H}_{12}^s \circ \mathbb{D}_{yy}) \\ \mathcal{B}_{12}^s \circ \mathbb{D}_x & \mathcal{B}_{22}^s \circ \mathbb{D}_y & -(\mathcal{D}_{12} \circ \mathbb{D}_{xx} + \mathcal{D}_{22} \circ \mathbb{D}_{yy}) & -(\mathcal{H}_{12}^s \circ \mathbb{D}_{xx} + \mathcal{H}_{22}^s \circ \mathbb{D}_{yy}) \\ \mathcal{B}_{66}^s \circ \mathbb{D}_y & \mathcal{B}_{66}^s \circ \mathbb{D}_x & -2\mathcal{D}_{66} \circ \mathbb{D}_{xy} & -2\mathcal{H}_{66}^s \circ \mathbb{D}_{xy} \end{bmatrix}$$

substituting Equation (22) into Equation (11) and applying DQM to discretize the governing differential equations into the following linear algebraic system

$$\begin{bmatrix} \mathbb{D}_x \mathcal{K}_{N_x} + \mathbb{D}_y \mathcal{K}_{N_{xy}} \\ \mathbb{D}_x \mathcal{K}_{N_{xy}} + \mathbb{D}_y \mathcal{K}_{N_y} \\ \mathbb{D}_{xx} \mathcal{K}_{M_x^b} + 2\mathbb{D}_{xy} \mathcal{K}_{M_{xy}^b} + \mathbb{D}_{yy} \mathcal{K}_{M_y^b} + K_p(\mathbb{D}_{xx} + \mathbb{D}_{yy}) - K_w I \\ \mathbb{D}_{xx} \mathcal{K}_{M_x^s} + 2\mathbb{D}_{xy} \mathcal{K}_{M_{xy}^s} + \mathbb{D}_{yy} \mathcal{K}_{M_y^s} + \mathbb{D}_y S_{yz}^s + \mathbb{D}_x S_{xz}^s + K_p(\mathbb{D}_{xx} + \mathbb{D}_{yy}) - K_w I \end{bmatrix}_{4mn \times 4mn} \mathcal{X} = F \tag{64}$$

where F is the force vector and

$$S_{yz}^s = [O \mathcal{A}_{44}^s \circ \mathbb{D}_y], \quad S_{xz}^s = [O \mathcal{A}_{55}^s \circ \mathbb{D}_x] \tag{65}$$

in which \mathbb{O} and \mathbb{I} are the zero and identity matrices of dimensions $(mn \times mn)$, respectively.

4. Problem Validation

The effect of the gradation index on the maximum static deflection and normal stress for the BDFG plate under uniform/sinusoidal transversal load based on neutral surface formulation (NS) is presented in Table 1. As shown, by increasing n_z , the material constituent changes from the ceramics phase (high stiffness) to graded phases to metal phase (low stiffness), hence, the static deflection and normal stress are increased. The same observations are predicted by Singha et al. [63] and Zenkour [64] as presented in Table 1. The obtained maximum deflection and normal stresses results are very close to that obtained by [63,64] for both uniform and Lateral sinusoidal loads.

Table 1. Comparison of the non-dimensional maximum deflection ($\bar{w} = w_{max} \frac{10Ech^3}{q_0a^4}$) and ($\bar{\sigma}_x = \frac{h}{aq_0} \sigma_x$) and ($\bar{\sigma}_x = \frac{h}{aq_0} \sigma_x$) of BDFG Al/Al₂O₃ square plate ($a/h = 10$) under uniform/sinusoidal transversal load based on neutral surface formulation (NS).

n_z	S_{im-NS}						C_{im-NS}		z_0/h	
	\bar{w}			$\bar{\sigma}_x$			\bar{w}		Present	Ref. [63]
	Present	Ref. [63]	Ref. [64]	Present	Ref. [63]	Ref. [64]	Present	Ref. [63]	Present	Ref. [63]
Uniformly distributed load										
ceramic	0.4665	0.4666	0.4665	2.8917	2.8688	2.8932	0.0013	0.0013	0	0
1	0.9287	0.9290	0.9287	4.4720	4.4303	4.4745	0.0025	0.0025	0.1148	0.1148
2	1.1939	1.1952	1.1940	5.2263	5.1689	5.2296	0.0033	0.0033	0.1490	0.1490
4	1.3882	1.3908	1.3890	5.8870	5.8035	5.8915	0.0037	0.0037	0.1566	0.1566
Metal	2.5326	-	2.5327	2.8917	-	2.8932	0.0069	0.0069	0	0
Lateral sinusoidal load										
ceramic	0.2961	0.2961	0.2960	1.9943	1.9679	1.9955	-	-	0	0
1	0.5890	0.5891	0.5889	3.0850	3.0389	3.0870	-	-	0.1148	0.1148
2	0.7573	0.7582	0.7573	3.6067	3.5456	3.6094	-	-	0.1490	0.1490
4	0.8815	0.8831	0.8819	4.0655	3.9813	4.0693	-	-	0.1566	0.1566
Metal	1.6072	1.6072	1.6070	1.9943	1.9679	1.9955	-	-	0	0

Figure 2 shows the variation of a transverse shear stress $\bar{\tau}_{xz}$ along the thickness direction for different elasticity ratios. As seen, the shear stress distribution has a parabolic

variation with zero values at the top and bottom surfaces. The results are identical with those obtained by [3], which confirms and validates the current model.

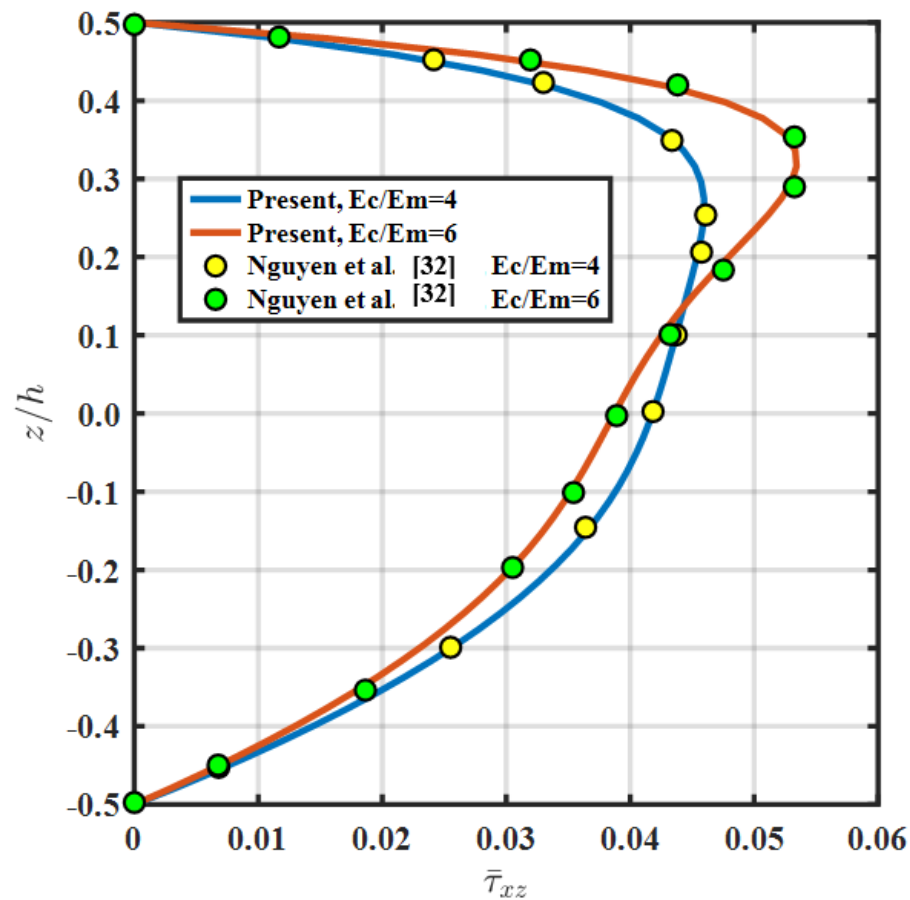


Figure 2. Non-dimensional stress ($\bar{\tau}_{xz} = \tau_{xz}h^2/a^2q_0$) at different Young’s modulus of ceramic and metal, E_c/E_m at ($a/h = 10$).

To verify the movable boundary conditions formulation, the current model is compared of the non-dimensional maximum deflection (\bar{w}) and stresses ($\bar{\sigma}_x, \bar{\sigma}_y, \bar{\tau}_{xy}, \bar{\tau}_{xz}$) of movable simply-supported BDFG Al/Al₂O₃ square plate ($a/h = 10$) under sinusoidal load based on neutral surface formulation (NS) with Mohamed et al. [65] as in Table 2. As concluded, the results for deflection and stresses at different gradation indices are very close to Mohamed’s results.

Table 2. Comparison of the non-dimensional maximum deflection ($\bar{w} = w_{max} \frac{10E_c h^3}{q_0 a^4}$) and stresses ($\bar{\sigma}_x, \bar{\sigma}_y, \bar{\tau}_{xy}, \bar{\tau}_{xz}$) of movable simply-supported (S_{m-NS}) BDFG Al/Al₂O₃ square plate ($a/h = 10$) under sinusoidal load based on neutral surface formulation (NS).

n_z	\bar{w}		$\bar{\sigma}_x$		$\bar{\sigma}_y$		$\bar{\tau}_{xy}$		$\bar{\tau}_{xz}$	
	Present	Ref. [65]	Present	Ref. [65]	Present	Ref. [65]	Present	Ref. [65]	Present	Ref. [65]
ceramic	0.2961	0.2960	1.9943	1.9952	1.3124	1.3122	0.7067	0.7066	0.2386	0.2441
0.2	0.3632	0.3599	2.2739	2.2600	1.3940	1.3871	0.7304	0.7205	0.2430	0.2481
0.5	0.4546	0.4537	2.6217	2.6193	1.4603	1.4586	0.6930	0.6912	0.2441	0.2495
1	0.5890	0.5889	3.0850	3.0864	1.4898	1.4895	0.6111	0.6111	0.2386	0.2441
2	0.7573	0.7573	3.6067	3.6086	1.3960	1.3956	0.5442	0.5441	0.2186	0.2243
5	0.9113	0.9117	4.2447	4.2476	1.1041	1.1033	0.5757	0.5755	0.1929	0.1992
Metal	1.6072	1.6071	1.9943	1.9952	1.3124	1.3122	0.7067	0.7066	0.2386	0.2441

Table 3 demonstrates the influences of elastic foundation parameters on the maximum deflection, normal stress, and shear stress of BDFG simply supported plates. As shown, by

increasing the shear stiffness of the elastic foundation from 0 to 100, the deflection, normal stress, and shear stress decreased by 11.2%, 11.5%, and 8.7%, respectively. This was due to increasing the stiffness of the structure by adding an elastic foundation constant. Results are very close to those obtained by Thai and Choi [66] and Zenkour and Sobhy [67] and deviated by 0.8% (for deflection), 3.3% (for normal stress), 2.0% (for shear stress) from the results obtained by Benahmed et al. [68] at $k_s = 100$ and $n_z = 0.5$.

Table 3. Comparison of the non-dimensional maximum deflection ($\bar{w} = w_{max} \frac{100E_c h^3}{12(1-\nu^2)q_0 a^4}$) and stresses ($\bar{\sigma}_x, \bar{\tau}_{xy}$) of movable simply supported (S_{m-NS}) BDFG Al/Al₂O₃ square plate ($a/h = 10$) under uniform load based on neutral surface formulation (NS) and foundations ($k_w = K_W a^4 / E_0 h^3$, $k_s = K_S a^2 / E_0 h^3 \nu$) and $E_0 = 1 GPa$.

n_z	k_w	k_s		\bar{w}	$\bar{\sigma}_x$	$\bar{\tau}_{xy}$
0.5	100	0	Present (S_{m-NS})	1.8624	0.2247	0.0911
			Ref [66]	1.8590	0.2242	0.0916
			Ref [67]	1.8591	0.2242	0.0917
			Ref [68]	1.8296	0.2299	0.0877
	100	100	Present (S_{m-NS})	1.6544	0.1988	0.0832
			Ref [66]	1.6640	0.1999	0.0850
			Ref [67]	1.6640	0.1999	0.0850
			Ref [68]	1.6414	0.2054	0.0815
5	100	0	Present (S_{m-NS})	3.5618	0.4816	0.1980
			Ref [66]	3.5620	0.4816	0.1996
			Ref [67]	3.5630	0.4817	0.1998
			Ref [68]	3.4286	0.4913	0.1845
	100	100	Present (S_{m-NS})	2.8689	0.3851	0.1678
			Ref [66]	2.9046	0.3897	0.1740
			Ref [67]	2.9052	0.3897	0.1741
			Ref [68]	2.8179	0.4006	0.1616

5. Numerical Results

The influence of (E_c / E_m) elasticity ratio on deflection and stresses for movable and immovable plates with different gradation indices and slenderness ratios are presented in Tables 4–6. As seen from Table 4, by increasing the gradation index or elasticity ratio, the deflection increases for both movable and immovable boundary conditions. However, increasing the slenderness ratio tends to decrease the deflection.

Table 4. Influence of Young’s modulus ratio (E_c / E_m) on the non-dimensional maximum deflection ($\bar{w} = w_{max} \frac{100E_c h^3}{12(1-\nu^2)q_0 a^4}$) of movable/immovable simply-supported BDFG Al/Al₂O₃ square plate ($a/h = 10, 100$) sinusoidal load based on neutral surface formulation (NS) at $n_x = 1$.

n_z	a/h	$E_c/E_m=2$				$E_c/E_m=4$				$E_c/E_m=6$			
		S_{m-MS}	S_{m-NS}	S_{im-MS}	S_{im-NS}	S_{m-MS}	S_{m-NS}	S_{im-MS}	S_{im-NS}	S_{m-MS}	S_{m-NS}	S_{im-MS}	S_{im-NS}
0.0	10	0.3657	0.3657	0.3657	0.3657	0.4528	0.4528	0.4528	0.4528	0.5022	0.5022	0.5022	0.5022
1		0.4417	0.4417	0.4379	0.4417	0.6709	0.6710	0.6472	0.6710	0.8259	0.8262	0.7791	0.8262
2		0.4615	0.4615	0.4569	0.4615	0.7487	0.7488	0.7137	0.7488	0.9716	0.9721	0.8930	0.9721
5		0.4819	0.4819	0.4790	0.4819	0.8202	0.8203	0.7924	0.8203	1.1021	1.1023	1.0297	1.1023
10		0.4982	0.4982	0.4968	0.4982	0.8762	0.8762	0.8608	0.8762	1.1951	1.1952	1.1505	1.1952
0.0	100	0.3464	0.3464	0.3464	0.3464	0.4280	0.4280	0.4280	0.4280	0.4745	0.4745	0.4745	0.4745
1		0.4187	0.4187	0.4149	0.4187	0.6376	0.6377	0.6139	0.6377	0.7865	0.7868	0.7397	0.7868
2		0.4366	0.4366	0.4320	0.4366	0.7088	0.7090	0.6738	0.7090	0.9217	0.9222	0.8430	0.9222
5		0.4547	0.4547	0.4518	0.4547	0.7706	0.7707	0.7428	0.7707	1.0335	1.0337	0.9611	1.0337
10		0.4703	0.4703	0.4689	0.4703	0.8225	0.8225	0.8072	0.8225	1.1173	1.1174	1.0729	1.1174

Table 5. Influence of Young’s modulus ratio (E_c/E_m) on the non-dimensional stress ($\bar{\sigma}_x = \frac{h^2}{a^2q} \sigma_x \left(\frac{a}{2}, \frac{b}{2}, \frac{h}{2}\right)$) of movable/immovable simply-supported BDFG Al/Al₂O₃ square plate ($a/h = 10,100$) sinusoidal load based on neutral surface formulation (NS) at $n_x = 1$.

n_z	a/h	$E_c/E_m=2$				$E_c/E_m=4$				$E_c/E_m=6$			
		S_{m-MS}	S_{m-NS}	S_{im-MS}	S_{im-NS}	S_{m-MS}	S_{m-NS}	S_{im-MS}	S_{im-NS}	S_{m-MS}	S_{m-NS}	S_{im-MS}	S_{im-NS}
0.0	10	0.1981	0.1981	0.1981	0.1981	0.1948	0.1948	0.1948	0.1948	0.1925	0.1925	0.1925	0.1925
1		0.2266	0.2266	0.2311	0.2273	0.2605	0.2605	0.2672	0.2641	0.2816	0.2817	0.2878	0.2880
2		0.2355	0.2355	0.2406	0.2360	0.2838	0.2838	0.2918	0.2876	0.3178	0.3180	0.3245	0.3259
5		0.2499	0.2499	0.2545	0.2501	0.3182	0.3182	0.3283	0.3206	0.3659	0.3659	0.3775	0.3719
10		0.2637	0.2637	0.2672	0.2638	0.3573	0.3573	0.3673	0.3584	0.4238	0.4238	0.4384	0.4271
0.0	100	0.1963	0.1963	0.1963	0.1963	0.1932	0.1932	0.1932	0.1932	0.1910	0.1910	0.1910	0.1910
1		0.2244	0.2244	0.2290	0.2252	0.2580	0.2581	0.2647	0.2616	0.2790	0.2791	0.2852	0.2854
2		0.2331	0.2331	0.2382	0.2337	0.2808	0.2808	0.2888	0.2846	0.3145	0.3147	0.3211	0.3226
5		0.2474	0.2474	0.2520	0.2476	0.3146	0.3146	0.3247	0.3169	0.3614	0.3614	0.3730	0.3674
10		0.2612	0.2612	0.2647	0.2613	0.3535	0.3535	0.3635	0.3546	0.4189	0.4190	0.4335	0.4222

Table 6. Influence of Young’s modulus ratio (E_c/E_m) on the non-dimensional stress ($\bar{\tau}_{xz} = \frac{h^2}{a^2q} \tau_{xz} \left(0, \frac{b}{2}, 0\right)$) of movable/immovable simply-supported BDFG Al/Al₂O₃ square plate ($a/h = 10,100$) sinusoidal load based on neutral surface formulation (NS) at $n_x = 1$.

n_z	a/h	$E_c/E_m=2$				$E_c/E_m=4$				$E_c/E_m=6$			
		S_{m-MS}	S_{m-NS}	S_{im-MS}	S_{im-NS}	S_{m-MS}	S_{m-NS}	S_{im-MS}	S_{im-NS}	S_{m-MS}	S_{m-NS}	S_{im-MS}	S_{im-NS}
0.0	10	0.2054	0.2054	0.2054	0.2054	0.1699	0.1699	0.1699	0.1699	0.1488	0.1488	0.1488	0.1488
1		0.2196	0.2196	0.2196	0.2196	0.1941	0.1941	0.1941	0.1941	0.1768	0.1768	0.1768	0.1768
2		0.2269	0.2269	0.2269	0.2269	0.2091	0.2091	0.2091	0.2091	0.1956	0.1956	0.1956	0.1956
5		0.2349	0.2349	0.2348	0.2349	0.2281	0.2281	0.2280	0.2281	0.2221	0.2221	0.2218	0.2221
10		0.2375	0.2375	0.2375	0.2375	0.2354	0.2354	0.2353	0.2354	0.2334	0.2334	0.2331	0.2334
0.0	100	0.2057	0.2057	0.2057	0.2057	0.1703	0.1703	0.1703	0.1703	0.1494	0.1494	0.1494	0.1494
1		0.2198	0.2198	0.2198	0.2198	0.1944	0.1944	0.1944	0.1944	0.1772	0.1772	0.1772	0.1772
2		0.2271	0.2271	0.2265	0.2271	0.2094	0.2094	0.2095	0.2094	0.1959	0.1959	0.2027	0.1959
5		0.2350	0.2350	0.2354	0.2350	0.2283	0.2283	0.2229	0.2283	0.2224	0.2224	0.2099	0.2224
10		0.2377	0.2377	0.2392	0.2377	0.2356	0.2356	0.2366	0.2356	0.2336	0.2336	0.2286	0.2336

From Table 4, due to bending–stretching uncoupling, one can notice that the transverse deflection of S_{m-NS} is identical with S_{im-NS} . For MS-formulation (the neutral is not included), the deflection of the immovable simply supported is less than the deflection of the NS formulation. This means that ignoring the effect of the neutral axis may result in underestimated deflections. However, from Table 5, the transverse deflection of S_{m-NS} is identical with S_{im-NS} , the stress $\bar{\sigma}_x$, which depends also on the values of u_0 and is not the same movable and immovable plates. In the immovable simply supported plate, $u_0 = v_0 = 0$, while in the movable plate, the plate has nonzero longitudinal deflections. It is noted that the normal and shear stresses are decreased by increasing the elasticity ratio (Tables 5 and 6). However, the slenderness ratio has no effect on the normal and shear stresses.

The effect of the elasticity ratio on the variables of the neutral axis with the variation of gradation index through the thickness direction is presented in Table 7. As shown, by increasing the gradation index from 0 to 2, the values of z_0/h and c_0/h are increased due to the variation from the ceramics (isotropic phase) to the FGM constituent. By increasing n_z from 2 to 10, the phase changes from FGM to metal (isotropic phase), hence, the mid-plane will be identical with the neutral and the neutral axis variables will be diminished until a value of zero.

Table 7. Maximum values of z_0/h and c_0/h at different n_z and E_c/E_m ratios ($n_x = 1$).

n_z	$E_c/E_m=2$		$E_c/E_m=4$		$E_c/E_m=6$	
	z_0/h	c_0/h	z_0/h	c_0/h	z_0/h	c_0/h
0.0	0.0000	0.0000	0.0000	0.0000	0.0000	0.0000
0.2	0.0214	0.0047	0.0337	0.0074	0.0381	0.0083
0.5	0.0401	0.0083	0.0669	0.0138	0.0772	0.0160
1	0.0556	0.0111	0.1000	0.0200	0.1190	0.0238
2	0.0625	0.0125	0.1250	0.0250	0.1563	0.0313
4	0.0556	0.0119	0.1250	0.0268	0.1667	0.0357
5	0.0510	0.0113	0.1190	0.0265	0.1623	0.0361
10	0.0347	0.0088	0.0893	0.0226	0.1303	0.0330

The variation of neutral axis variables with elastic ratio is presented in Figure 3 at $n_z = 2$ and $n_x = 1$. The parabolic increasing of z_0/h and c_0/h are observed by increasing the elasticity ratio. So that, the distance between mid-plane and neutral axis increased. Hence, the accurate results should be evaluated with respect to neutral surface rather than mid-plane specially for higher elasticity ratio. The same observations are predicted for the variation of gradation indices n_z and n_x as seen in Figures 4 and 5, respectively.

Influences of the gradation n_x and n_z for a different a/h – ratio on \bar{w} , $\bar{\sigma}_x$, $\bar{\tau}_{xy}$, $\bar{\tau}_{xz}$ for immovable BDFG Al/Al₂O₃ square plate at specified points a uniform distributed load are presented in Table 7. The quantitative analysis of Table 8 is portrayed in the 3D plots shown in Figure 6. As shown, the highlights deflection and shear stresses are obtained for higher gradation indices; however, the higher normal stress is obtained at $n_z = 3$ and $n_x = 0$, as seen in Figure 6.

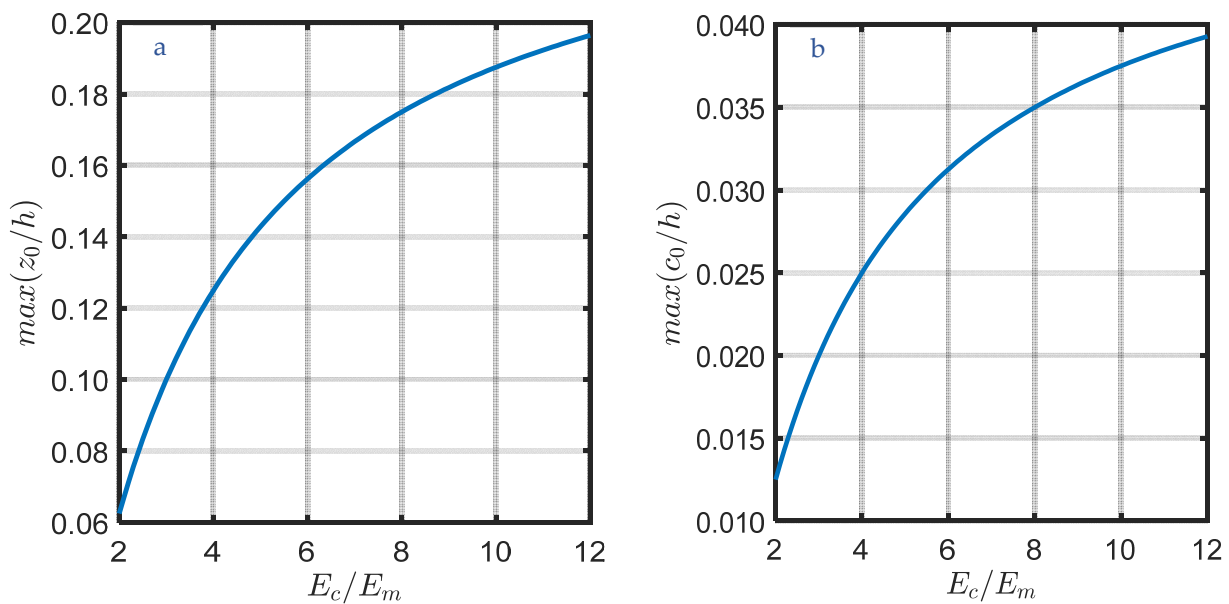


Figure 3. Maximum values of (a) z_0/h and (b) c_0/h at different E_c/E_m ratios at ($n_z = 2$, $n_x = 1$).

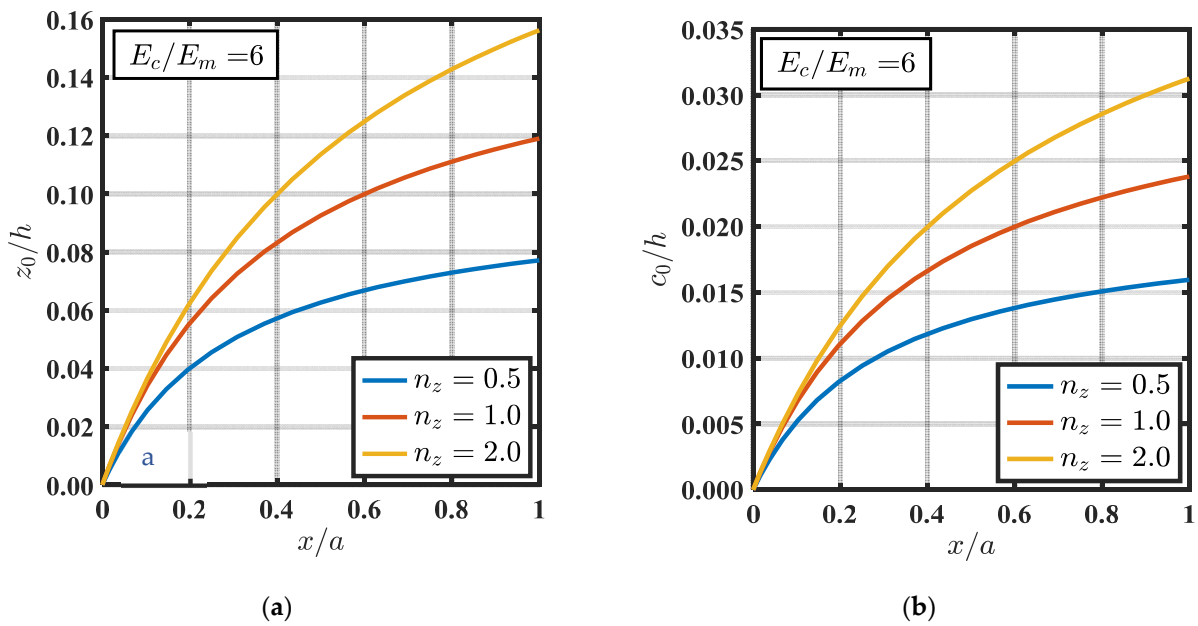


Figure 4. Neutral axis paramaters z_0/h and c_0/h at different n_z and young's modulus of ceramic and metal, $E_c/E_m = 6$ at ($a/h = 10, n_x = 1$) (a) for z_0/h and (b) for c_0/h .

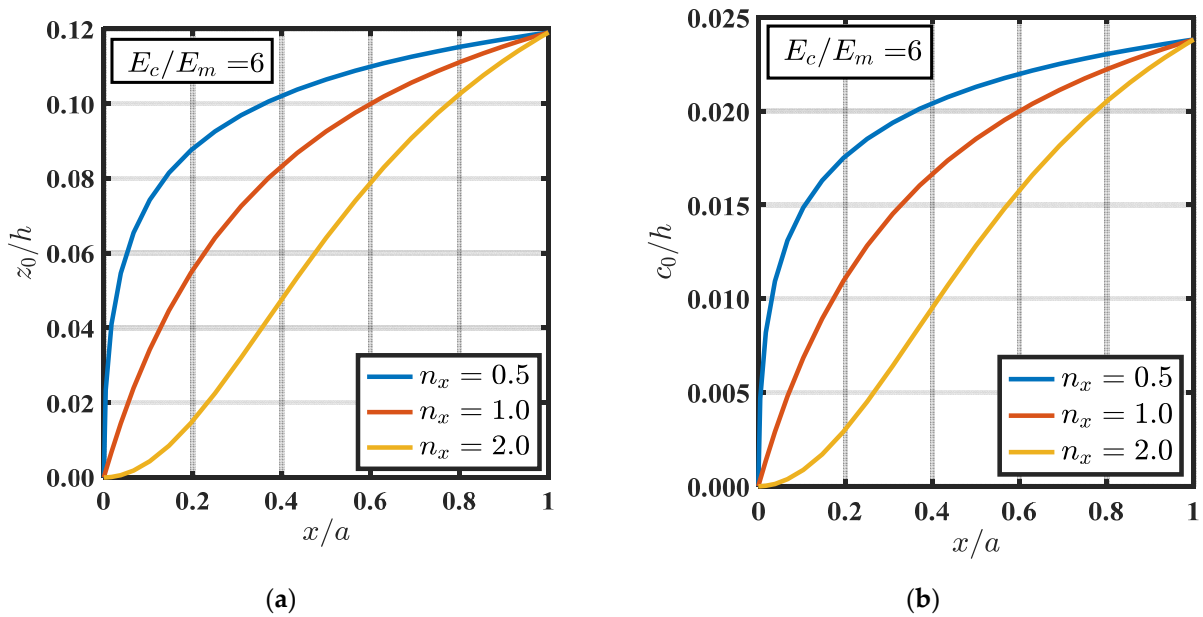


Figure 5. Neutral axis paramaters z_0/h and c_0/h at different n_x and young's modulus of ceramic and metal, $E_c/E_m = 6$ at ($a/h = 10, n_z = 1$) (a) for z_0/h and (b) for c_0/h .

Table 8. Influence of gradation indices on the non-dimensional maximum deflection ($\bar{w} = w_{max} \frac{100E_c h^3}{12(1-\nu^2)q_0 a^4}$) and different stresses of immovable BDFG Al/Al₂O₃ square plate ($a/h = 10, 100$) uniform load based on neutral surface formulation (NS) formulation. $\bar{\sigma}_x = \frac{h^2}{a^2 q^2} \sigma_x \left(\frac{a}{2}, \frac{b}{2}, \frac{h}{2}\right)$, $\bar{\tau}_{xy} = \frac{h^2}{a^2 q} \tau_{xy} \left(0, 0, -\frac{h}{3}\right)$, $\bar{\tau}_{xz} = \frac{h^2}{a^2 q} \tau_{xz} \left(0, \frac{b}{2}, 0\right)$.

n_z		\bar{w}	$\bar{\sigma}_x$	$\bar{\tau}_{xy}$	$\bar{\tau}_{xz}$	\bar{w}	$\bar{\sigma}_x$	$\bar{\tau}_{xy}$	$\bar{\tau}_{xz}$
		$n_x = 0.5$				$n_x = 1$			
0.5	$a/h = 10$	0.8359	0.3876	0.0556	0.2630	1.0313	0.3630	0.0737	0.3625
1		0.9925	0.4481	0.0636	0.2987	1.1752	0.4111	0.0802	0.3848
2		1.1584	0.5105	0.0709	0.3530	1.3299	0.4599	0.0864	0.4163
5		1.3570	0.5983	0.0799	0.4302	1.5183	0.5316	0.0946	0.4578
		$n_x = 2$				$n_x = 5$			
0.5	$a/h = 100$	1.3514	0.3202	0.0943	0.3989	1.7829	0.2707	0.1122	0.4430
1		1.4691	0.3517	0.0991	0.4150	1.8690	0.2803	0.1148	0.4508
2		1.5898	0.3820	0.1034	0.4374	1.9466	0.2887	0.1171	0.4616
5		1.7444	0.4268	0.1087	0.4663	2.0361	0.2993	0.1197	0.4750
		$n_x = 0.5$				$n_x = 1$			
0.5	$a/h = 100$	0.7977	0.3852	0.0561	0.2540	0.9809	0.3609	0.0745	0.3536
1		0.9464	0.4452	0.0643	0.3001	1.1198	0.4086	0.0811	0.3862
2		1.0981	0.5069	0.0718	0.3724	1.2607	0.4568	0.0874	0.4264
5		1.2704	0.5933	0.0811	0.4139	1.4261	0.5273	0.0957	0.4413
		$n_x = 2$				$n_x = 5$			
0.5	$a/h = 100$	1.2851	0.3184	0.0952	0.3903	1.6984	0.2687	0.1132	0.4323
1		1.3958	0.3494	0.1001	0.4160	1.7793	0.2783	0.1158	0.4519
2		1.5088	0.3793	0.1044	0.4468	1.8497	0.2866	0.1181	0.4811
5		1.6458	0.4235	0.1098	0.4561	1.9300	0.2972	0.1208	0.4722

The variations of normal and shear stresses across the thickness direction with respect to the gradation indices n_z and n_x are illustrated in Figures 7 and 8. As shown, the gradation index n_z tends to change the distribution profiles of the stresses along the thickness directions; however, the gradation index n_x has no effect on the distribution profiles but has an effect on the peaks.

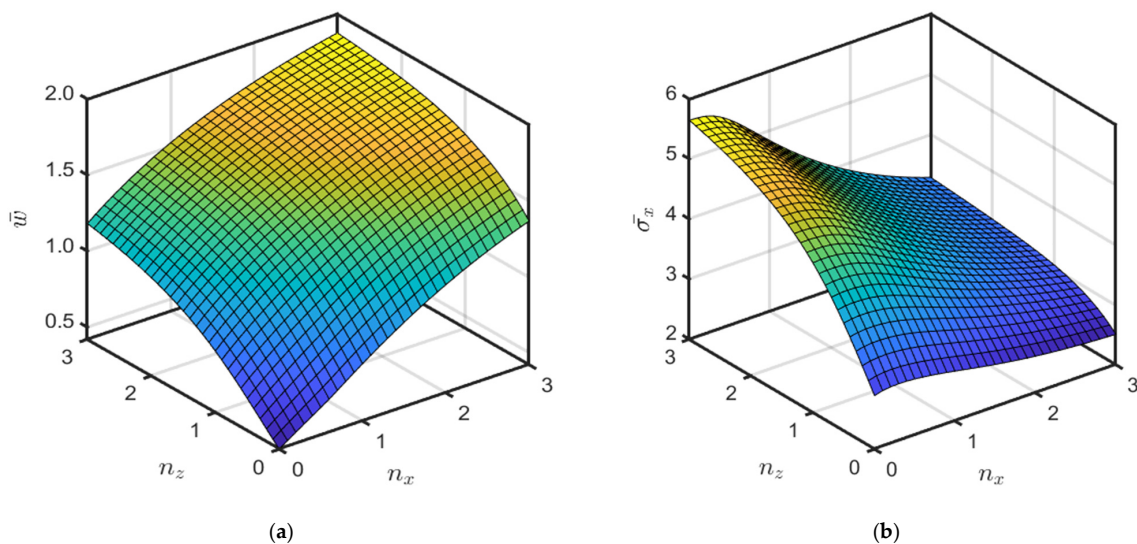


Figure 6. Cont.

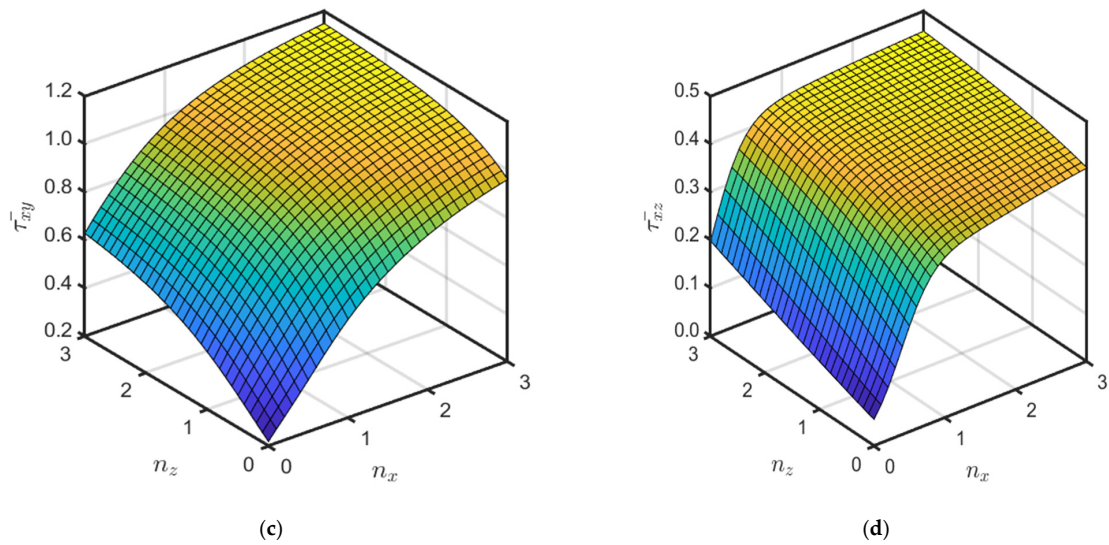


Figure 6. Effect of gradation indices on the non-dimensional maximum deflection ($\bar{w} = w_{max} \frac{100E_c h^3}{12(1-\nu^2)q_0 a^4}$) and stresses of (S_{im-NS}) BDFG under sinusoidal load ($a/h = 10$). (a) Maximum deflection. (b) Normal stress $\bar{\sigma}_x$. (c) Shear stress $\bar{\tau}_{xy}$. (d) Shear stress $\bar{\tau}_{xz}$.

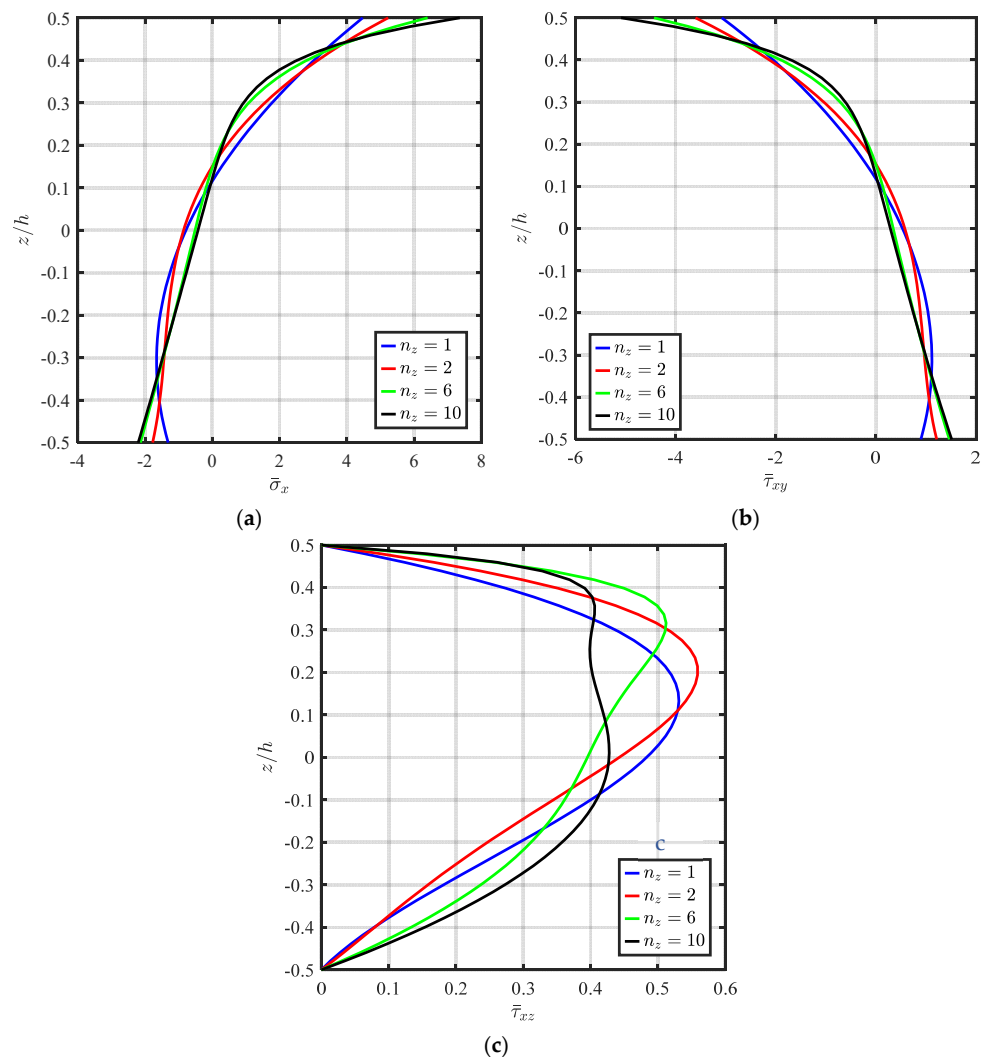


Figure 7. Non-dimensional stresses of (S_{im-NS}) BDFG at different n_z ($a/h = 10, n_x = 0$). (a) Normal stress $\bar{\sigma}_x$. (b) Shear stress $\bar{\tau}_{xy}$. (c) Shear stress $\bar{\tau}_{xz}$.

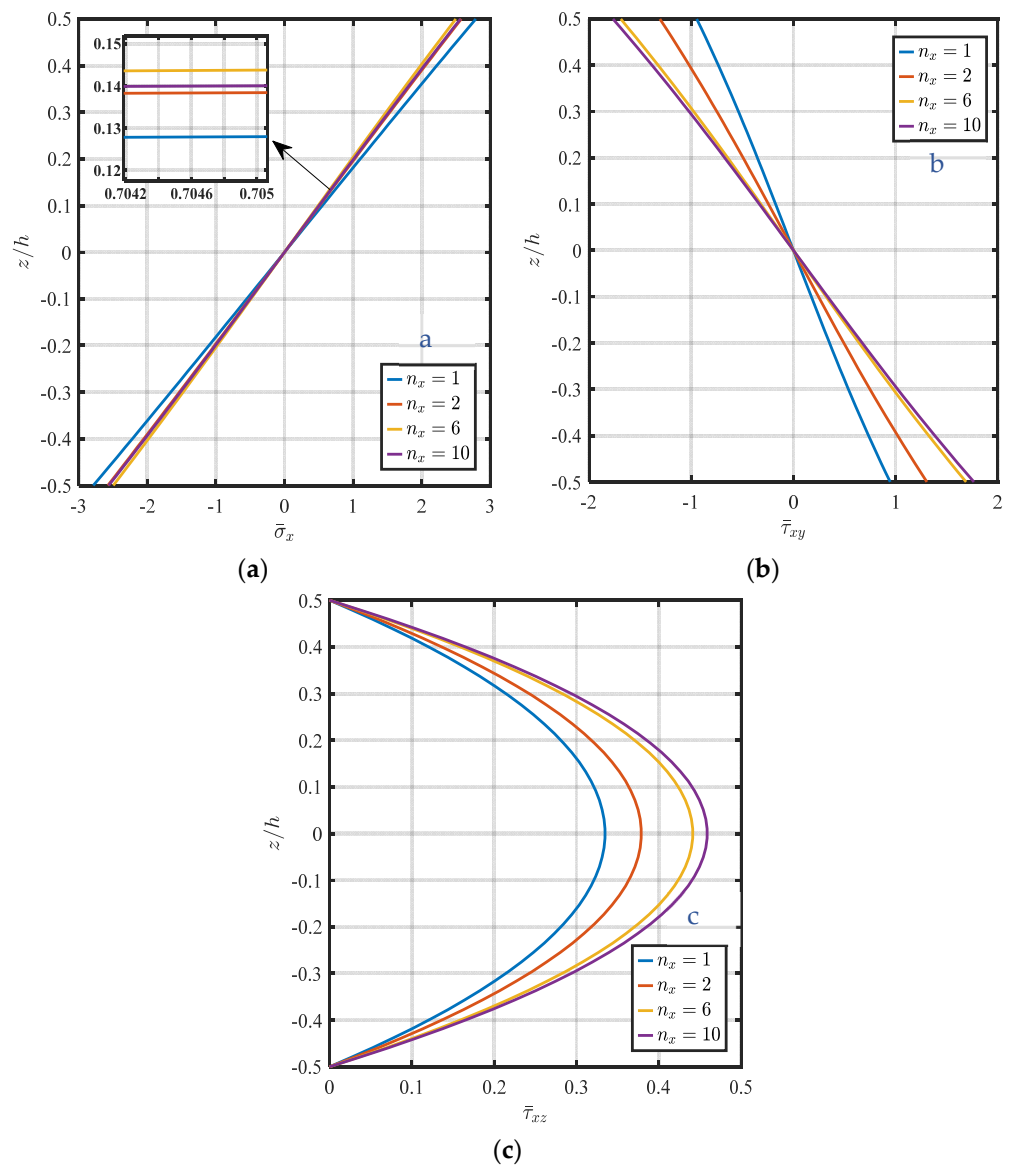


Figure 8. Non-dimensional stresses of (S_{im-NS}) BDFG at different n_x ($a/h = 10$, $n_z = 0$). (a) Normal stress $\bar{\sigma}_x$. (b) Shear stress $\bar{\tau}_{xy}$. (c) Shear stress $\bar{\tau}_{xz}$.

The variation of the deflection with plate aspect ratio b/a for both simply supported and clamped boundary conditions under a uniform load is presented in Figure 9. The movable/immovable boundary conditions and mid-plane/neutral surface are considered. As shown, the maximum deflection increased linearly with an increasing plate aspect ratio b/a for simply supported boundary conditions. However, in the case of a clamped boundary condition, the deflection increased linearly in as b/a changes from 0.5 to 1.5, and after that, the effect of the aspect ratio on the maximum deflection decreased.

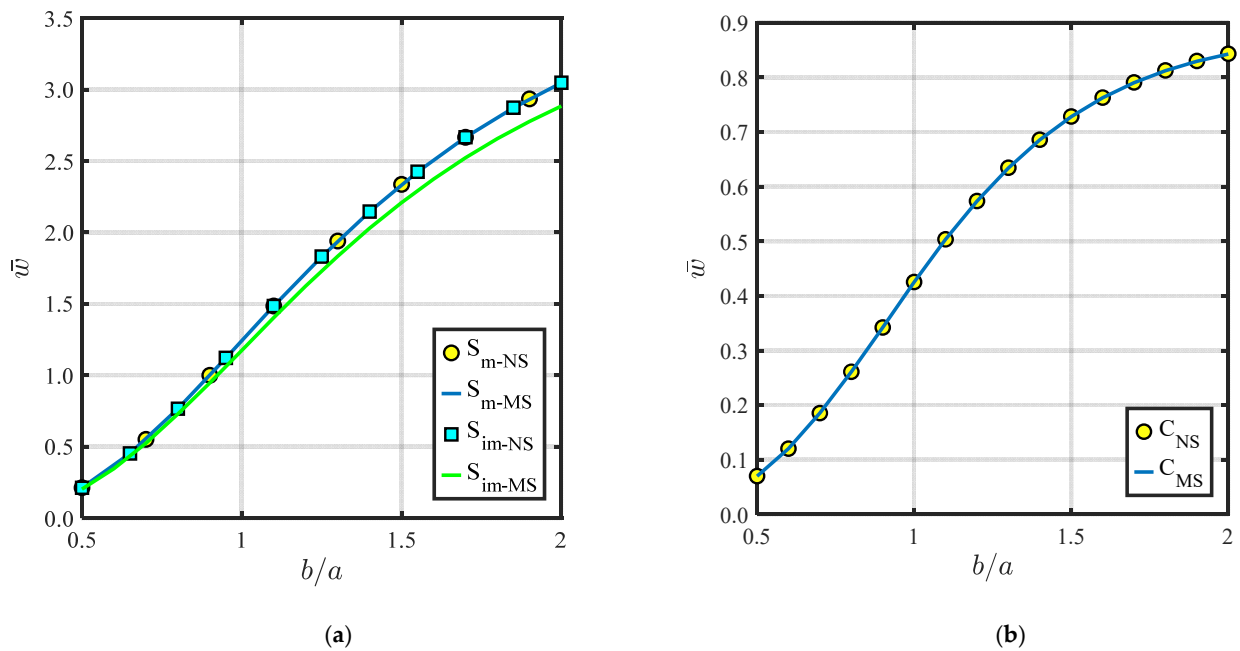


Figure 9. Non-dimensional maximum deflection ($\bar{w} = w_{max} \frac{100E_c h^3}{12(1-\nu^2)q_0 a^4}$) of BDFG under uniform load at different aspect ratio b/a , ($a/h = 10$, $n_x = n_z = 1$). (a) Simply supported. (b) Fully Clamped.

The effect of the porosity coefficient of a type one on the deflection for both simply supported and clamped boundary conditions is presented in Figure 10. As shown, by increasing the porosity parameter, the deflection increases due to reducing the overall stiffness of the structure. The immovable boundary condition relative to MS is smaller than S_{m-NS} , S_{m-MS} , and S_{im-NS} cases for simply supported boundary conditions.

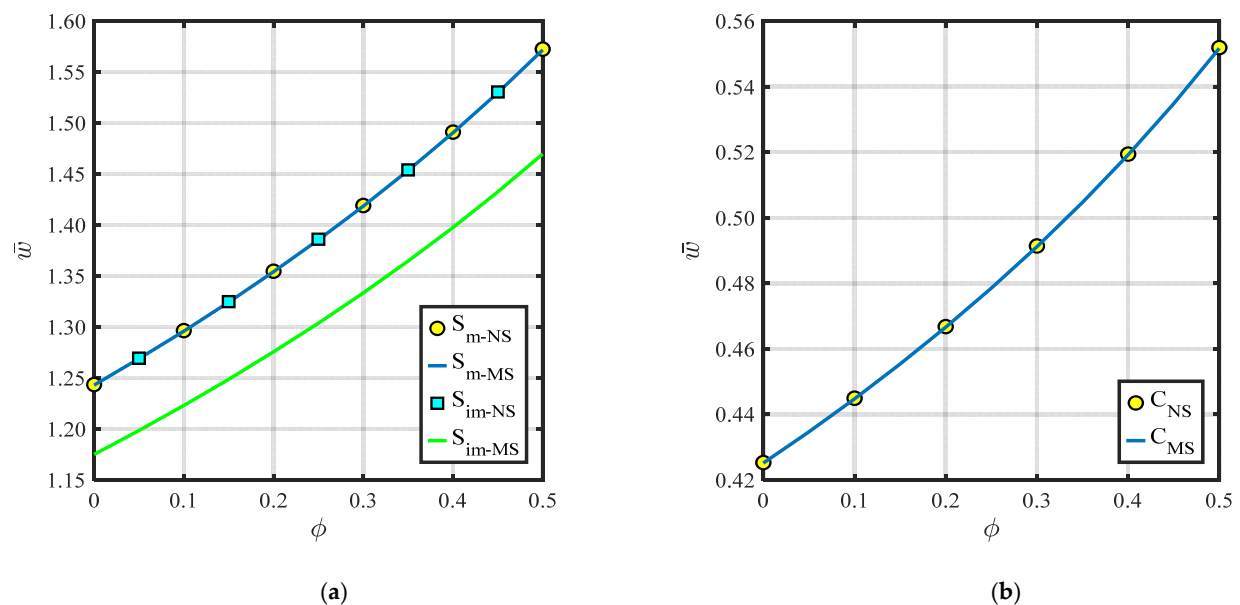


Figure 10. Non-dimensional maximum deflection ($\bar{w} = w_{max} \frac{100E_c h^3}{12(1-\nu^2)q_0 a^4}$) of BDFG under uniform load at a different porosity parameter ϕ (type 1), ($a/h = 10$, $n_x = n_z = 1$). (a) Simply Supported. (b) Fully clamped.

Effects of elastic foundation parameters (K_w and K_s) on \bar{w} , $\bar{\sigma}_x$, $\bar{\tau}_{xy}$, $\bar{\tau}_{xz}$ at specified points for A movable/immovable, Al/Al₂O₃, (FGM), square plate, subjected to uniform loading, using NS formulation, $n_x = n_z = 1$, $a/h = 10$ are presented in Figures 11–14. As seen, by increasing the elastic foundation constants, the deflection, normal stress, and shear

stresses are decreased linearly with respect to k_w and parabolically with respect to k_p for simply supported BCs. It is also noted that the effects of MS/NS and movable/immovable boundary conditions have significant influences on the stresses and maximum deflection.

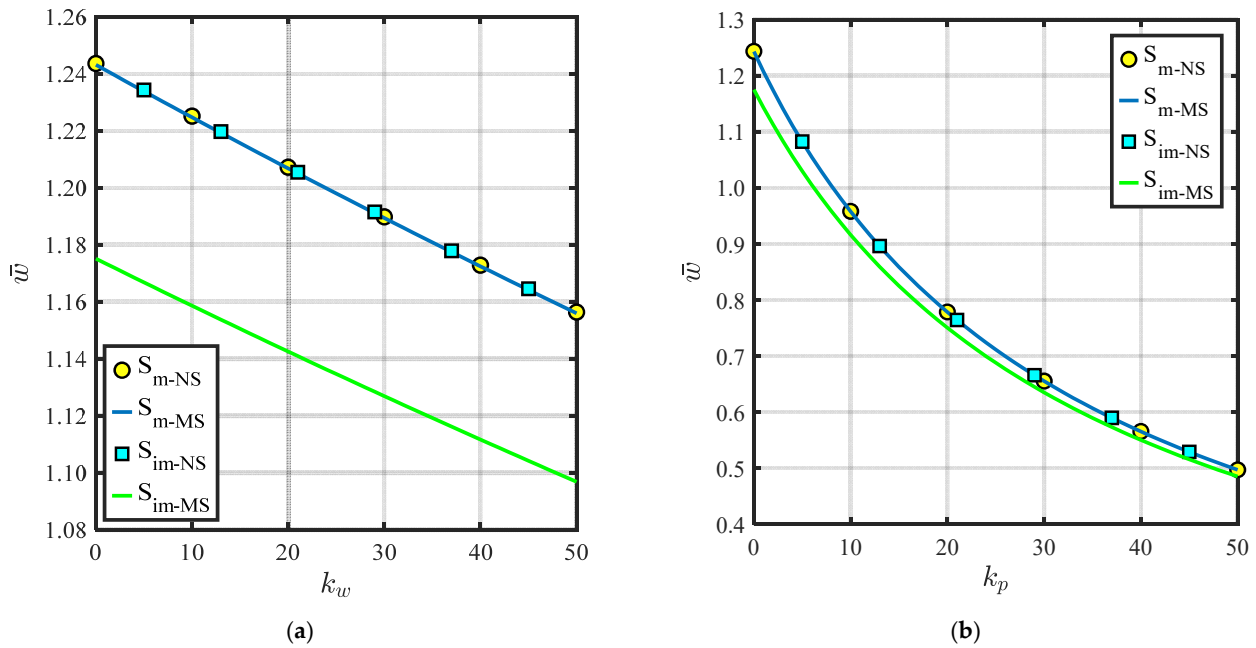


Figure 11. Maximum deflection \bar{w} of BDFG under uniform load at $(a/h = 10, n_x = n_z = 1)$ for different k_w and k_p . (a) For different k_w . (b) For different k_p .

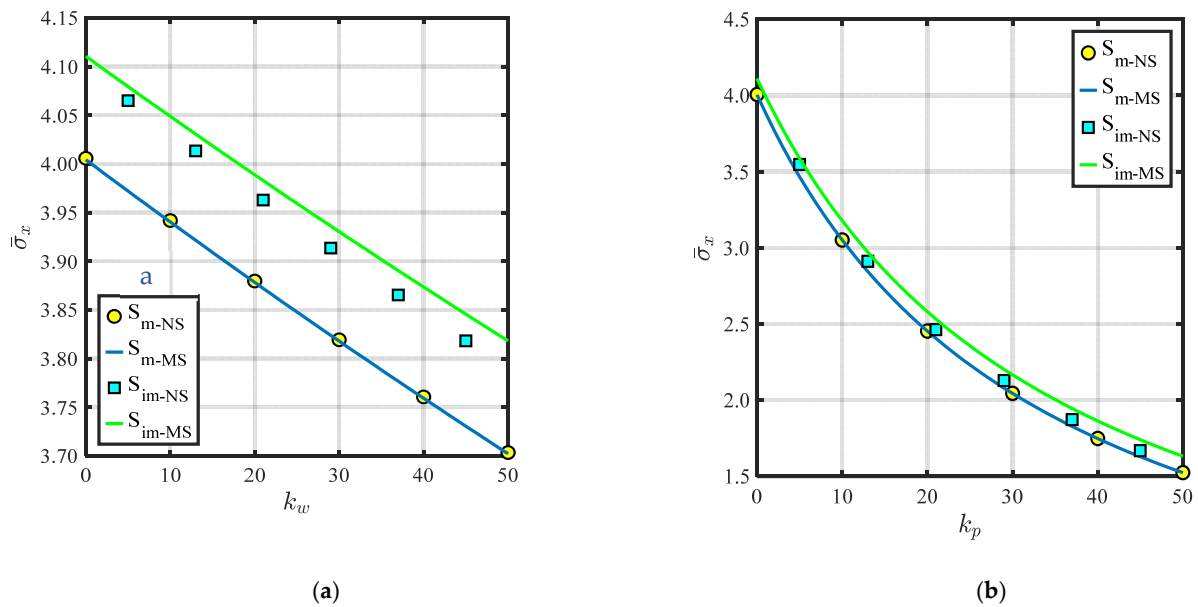


Figure 12. Normal stress $\bar{\sigma}_x = \frac{h}{aq} \sigma_x \left(\frac{a}{2}, \frac{b}{2}, \frac{h}{2} \right)$ of BDFG under uniform load at $a/h = 10, n_x = n_z = 2$ for different k_w and k_p . (a) For different k_w . (b) For different k_p .

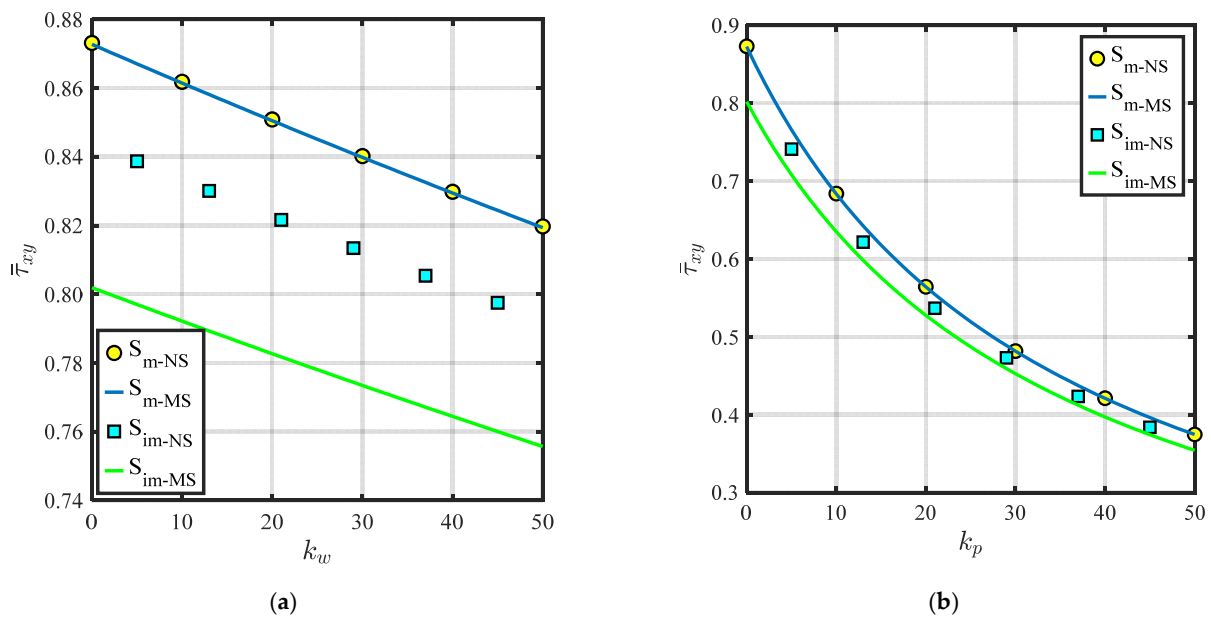


Figure 13. Shear stress $\bar{\tau}_{xy} = \frac{h}{aq} \tau_{xy} \left(0, 0, -\frac{h}{3} \right)$ of BDFG under uniform load at $a/h = 10$, $n_x = n_z = 2$ for different k_w and k_p . (a) For different k_w . (b) For different k_p .

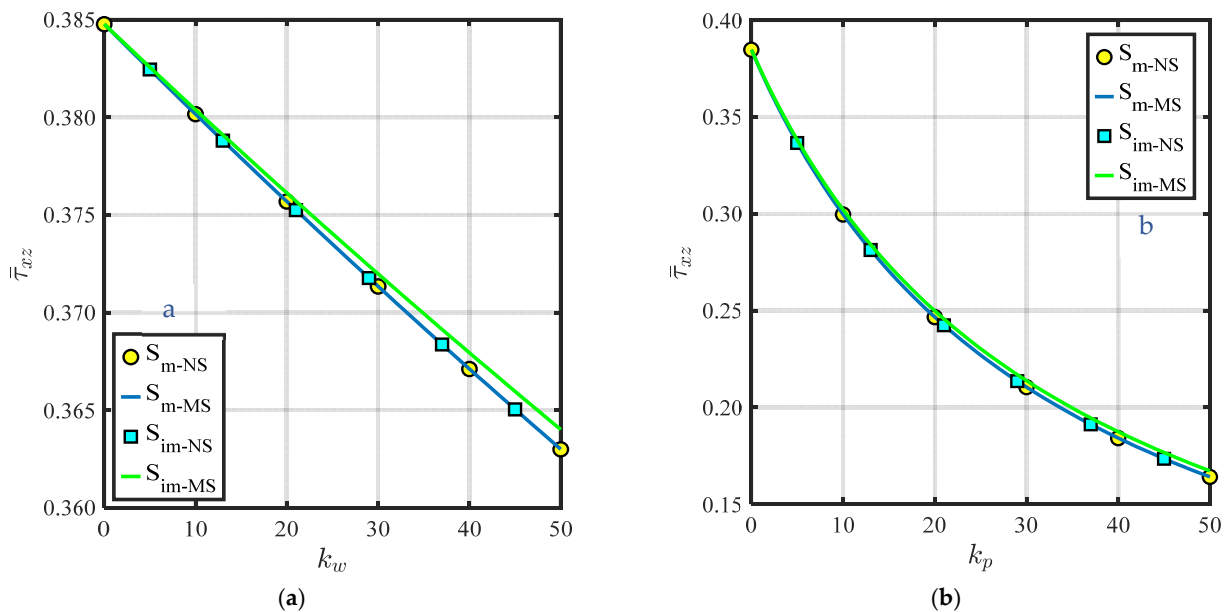


Figure 14. Shear stress $\bar{\tau}_{xz} = \frac{h}{aq} \tau_{xz} \left(0, 0, -\frac{h}{3} \right)$ of BDFG under uniform load at $a/h = 10$, $n_x = n_z = 2$ for different k_w and k_p . Conclusion. (a) For different k_w . (b) For different k_p .

Mathematical and numerical formulations are developed to investigate the bending and the stress variation of the BDFG porous plate with elastic foundations. Bi-directional gradations are defined by power function; however, porosity distribution is defined by cosine function. The influence of middle surface (MS), neutral surface (NS), movable BCs, and immovable BCs are considered in the formulation. Elastic foundation is portrayed by the Winkler–Pasternak model. The equilibrium equations are derived by Hamilton’s principles and then solved numerically by using the discretized by differential quadrature method (DQM). The main points of the present study can be stated as follows:

- By increasing the gradation index or elasticity ratio, the deflection increases for both movable and immovable boundary conditions.
- Increasing of the slenderness ratio tends to decrease the deflection.

- It is expected that due to bending–stretching uncoupling, the transverse deflection of S_{m-NS} is identical with S_{im-NS} .
- For MS formulation (the neutral is not included), the deflection of immovable simply supported is less than the deflection of NS formulation.
- By increasing the gradation index from 0 to 2, the values of z_0/h and c_0/h are increased due to the variation from ceramics (isotropic phase) to FGM constituent.
- By increasing n_z from 2 to 10, the phase changes from FGM to metal (isotropic phase), hence, the mid-plane will be identical with the neutral and the neutral axis variables will be diminished until a value of zero.
- The parabolic increasing of z_0/h and c_0/h are observed by increasing the elasticity ratio.
- The gradation index n_z tends to change the distribution profiles of the stresses along the thickness directions, however, the gradation index n_x has no effect on the distribution profiles but influences the peaks.
- By increasing the porosity parameter, the deflection increases due to reducing the overall stiffness of the structure.
- By increasing the elastic foundation constants, the deflection, normal stress, and shear stresses are decreased linearly with respect to k_w and parabolically with respect to k_p .

Author Contributions: A.M. (project administration, funding acquisition, data curation, resources); S.A.M. (software, validation, formal analysis, investigation, original draft); A.E.A. (formal analysis, investigation, resources, original draft); R.A.S. (software, visualization, data curation, formal analysis); M.A.E. (Conceptualization, methodology, review and editing). All authors have read and agreed to the published version of the manuscript.

Funding: This research was funded by Ministry of Education and King Abdulaziz University, DSR in Jeddah grant no. IFPIP (1683-135-1443).

Data Availability Statement: Not applicable.

Acknowledgments: The authors gratefully acknowledge technical and financial support provided by the Ministry of Education and King Abdulaziz University, DSR in Jeddah, Saudi Arabia.

Conflicts of Interest: The authors declare no conflict of interest.

References

1. Su, J.; He, W.; Zhou, K. Study on vibration behavior of functionally graded porous material plates immersed in liquid with general boundary conditions. *Thin-Walled Struct.* **2023**, *182*, 110166. [\[CrossRef\]](#)
2. Alshorbagy, A.E.; Eltaher, M.A.; Mahmoud, F. Free vibration characteristics of a functionally graded beam by finite element method. *Appl. Math. Model.* **2011**, *35*, 412–425. [\[CrossRef\]](#)
3. Nguyen, V.D.; Phung, V.B. Static bending, free vibration, and buckling analyses of two-layer FGM plates with shear connectors resting on elastic foundations. *Alex. Eng. J.* **2023**, *62*, 369–390. [\[CrossRef\]](#)
4. Assie, A.E.; Mohamed, S.M.; Shanab, R.A.; Abo-bakr, R.M.; Eltaher, M.A. Static Buckling of 2D FG Porous Plates Resting on Elastic Foundation based on Unified Shear Theories. *J. Appl. Comput. Mech.* **2023**, *9*, 239–258. [\[CrossRef\]](#)
5. Shanab, R.A.; Attia, M.A. Semi-analytical solutions for static and dynamic responses of bi-directional functionally graded nonuniform nanobeams with surface energy effect. *Eng. Comput.* **2022**, *38*, 2269–2312. [\[CrossRef\]](#)
6. Nemat-Alla, M. Reduction of thermal stresses by developing two-dimensional functionally graded materials. *Int. J. Solids Struct.* **2003**, *40*, 7339–7356. [\[CrossRef\]](#)
7. Lü, C.F.; Lim, C.W.; Chen, W.Q. Semi-analytical analysis for multi-directional functionally graded plates: 3-D elasticity solutions. *Int. J. Numer. Methods Eng.* **2009**, *79*, 25–44. [\[CrossRef\]](#)
8. Bediz, B. Three-dimensional vibration behavior of bi-directional functionally graded curved parallelepipeds using spectral Tchebychev approach. *Compos. Struct.* **2018**, *191*, 100–112. [\[CrossRef\]](#)
9. Esmaeilzadeh, M.; Kadkhodayan, M. Dynamic analysis of stiffened bi-directional functionally graded plates with porosities under a moving load by dynamic relaxation method with kinetic damping. *Aerosp. Sci. Technol.* **2019**, *93*, 105333. [\[CrossRef\]](#)
10. Esmaeilzadeh, M.; Golmakani, M.E.; Luo, Y.; Bodaghi, M. Transient behavior of imperfect bi-directional functionally graded sandwich plates under moving loads. *Eng. Comput.* **2021**, 1–11. [\[CrossRef\]](#)
11. Ghatage, P.S.; Kar, V.R.; Sudhagar, P.E. On the numerical modelling and analysis of multi-directional functionally graded composite structures: A review. *Compos. Struct.* **2020**, *236*, 111837. [\[CrossRef\]](#)
12. Do, D.T.; Nguyen-Xuan, H.; Lee, J. Material optimization of tri-directional functionally graded plates by using deep neural network and isogeometric multimesh design approach. *Appl. Math. Model.* **2020**, *87*, 501–533. [\[CrossRef\]](#)

13. Qin, Z.; Chu, F.; Zu, J. Free vibrations of cylindrical shells with arbitrary boundary conditions: A comparison study. *Int. J. Mech. Sci.* **2017**, *133*, 91–99. [[CrossRef](#)]
14. Qin, Z.; Pang, X.; Safaei, B.; Chu, F. Free vibration analysis of rotating functionally graded CNT reinforced composite cylindrical shells with arbitrary boundary conditions. *Compos. Struct.* **2019**, *220*, 847–860. [[CrossRef](#)]
15. Qin, Z.; Zhao, S.; Pang, X.; Safaei, B.; Chu, F. A unified solution for vibration analysis of laminated functionally graded shallow shells reinforced by graphene with general boundary conditions. *Int. J. Mech. Sci.* **2020**, *170*, 105341. [[CrossRef](#)]
16. Karamanli, A.; Aydogdu, M.; Vo, T.P. A comprehensive study on the size-dependent analysis of strain gradient multi-directional functionally graded microplates via finite element model. *Aerosp. Sci. Technol.* **2021**, *111*, 106550. [[CrossRef](#)]
17. Eltaher, M.A.; Fouda, N.; El-midany, T.; Sadoun, A.M. Modified porosity model in analysis of functionally graded porous nanobeams. *J. Braz. Soc. Mech. Sci. Eng.* **2018**, *40*, 141. [[CrossRef](#)]
18. Li, S.; Zheng, S.; Chen, D. Porosity-dependent isogeometric analysis of bi-directional functionally graded plates. *Thin-Walled Struct.* **2020**, *156*, 106999. [[CrossRef](#)]
19. Genao, F.Y.; Kim, J.; Zur, K.K. Nonlinear finite element analysis of temperature-dependent functionally graded porous micro-plates under thermal and mechanical loads. *Compos. Struct.* **2021**, *256*, 112931. [[CrossRef](#)]
20. Hamed, M.A.; Abo-Bakr, R.M.; Mohamed, S.A.; Eltaher, M.A. Influence of axial load function and optimization on static stability of sandwich functionally graded beams with porous core. *Eng. Comput.* **2020**, *36*, 1929–1946. [[CrossRef](#)]
21. Li, J.; Wang, G.; Guan, Y.; Zhao, G.; Lin, J.; Naceur, H.; Coutellier, D. Meshless analysis of bi-directional functionally graded beam structures based on physical neutral surface. *Compos. Struct.* **2021**, *259*, 113502. [[CrossRef](#)]
22. Gao, W.; Liu, Y.; Qin, Z.; Chu, F. Wave Propagation in Smart Sandwich Plates with Functionally Graded Nanocomposite Porous Core and Piezoelectric Layers in Multi-Physics Environment. *Int. J. Appl. Mech.* **2022**, *14*, 2250071. [[CrossRef](#)]
23. Bekkaye, T.H.L.; Fahsi, B.; Bousahla, A.A.; Bourada, F.; Tounsi, A.; Benrahou, K.H.; Al-Zahrani, M.M. Porosity-dependent mechanical behaviors of FG plate using refined trigonometric shear deformation theory. *Comput. Concr.* **2020**, *26*, 439–450. [[CrossRef](#)]
24. Akbaş, Ş.D.; Fageehi, Y.A.; Assie, A.E.; Eltaher, M.A. Dynamic analysis of viscoelastic functionally graded porous thick beams under pulse load. *Eng. Comput.* **2022**, *38*, 365–377. [[CrossRef](#)]
25. Akbaş, Ş.D.; Bashiri, A.H.; Assie, A.E.; Eltaher, M.A. Dynamic analysis of thick beams with functionally graded porous layers and viscoelastic support. *J. Vib. Control* **2021**, *27*, 1644–1655. [[CrossRef](#)]
26. Ramteke, P.M.; Panda, S.K.; Patel, B. Nonlinear eigenfrequency characteristics of multi-directional functionally graded porous panels. *Compos. Struct.* **2022**, *279*, 114707. [[CrossRef](#)]
27. Ghandourah, E.E.; Daikh, A.A.; Alhawsawi, A.M.; Fallatah, O.A.; Eltaher, M.A. Bending and Buckling of FG-GRNC Laminated Plates via Quasi-3D Nonlocal Strain Gradient Theory. *Mathematics* **2022**, *10*, 1321. [[CrossRef](#)]
28. Khadir, A.I.; Daikh, A.A.; Eltaher, M.A. Novel four-unknowns quasi 3D theory for bending, buckling and free vibration of functionally graded carbon nanotubes reinforced composite laminated nanoplates. *Adv. Nano Res.* **2021**, *11*, 621–640. [[CrossRef](#)]
29. Kabouche, A.; Bachir Bouiadja, R.; Bachiri, A.; Sekkal, M.; Benyoucef, S.; Saleh, M.M.S.; Tounsi, A.; Hussain, M. Study on the Mechanical Instability of Bidirectional Imperfect FG Sandwich Plates Subjected to In-Plane Loading. *Arab. J. Sci. Eng.* **2022**, *47*, 13655–13672. [[CrossRef](#)]
30. Thi, H.N. Thermal vibration analysis of functionally graded porous plates with variable thickness resting on elastic foundations using finite element method. *Mech. Based Des. Struct. Mach.* **2022**, *1–29*. [[CrossRef](#)]
31. Mohamed, N.; Eltaher, M.A.; Mohamed, S.A.; Seddek, L.F. Numerical analysis of nonlinear free and forced vibrations of buckled curved beams resting on nonlinear elastic foundations. *Int. J. Non-Linear Mech.* **2018**, *101*, 157–173. [[CrossRef](#)]
32. Nguyen Thi, H. Free vibration and static bending analysis of piezoelectric functionally graded material plates resting on one area of two-parameter elastic foundation. *Math. Probl. Eng.* **2020**. [[CrossRef](#)]
33. Phuc, P.M.; Kim Khue, N.T. New finite modeling of free and forced vibration responses of piezoelectric FG plates resting on elastic foundations in thermal environments. *Shock Vib.* **2021**. [[CrossRef](#)]
34. Mohamed, S.A.; Mohamed, N.; Eltaher, M.A. Snap-through instability of helicoidal composite imperfect beams surrounded by nonlinear elastic foundation. *Ocean Eng.* **2022**, *263*, 112171. [[CrossRef](#)]
35. Almitani, K.H.; Mohamed, N.; Alazwari, M.A.; Mohamed, S.A.; Eltaher, M.A. Exact Solution of Nonlinear Behaviors of Imperfect Bioinspired Helicoidal Composite Beams Resting on Elastic Foundations. *Mathematics* **2022**, *10*, 887. [[CrossRef](#)]
36. Mohamed, N.; Mohamed, S.A.; Eltaher, M.A. Nonlinear Static Stability of Imperfect Bio-Inspired Helicoidal Composite Beams. *Mathematics* **2022**, *10*, 1084. [[CrossRef](#)]
37. Hashemi, S.; Shahri, P.K.; Beigzadeh, S.; Zamani, F.; Eratbeni, M.G.; Mahdavi, M.; Heidari, A.; Khaledi, H.; Abadi, M.R.R. Nonlinear free vibration analysis of In-plane Bi-directional functionally graded plate with porosities resting on elastic foundations. *Int. J. Appl. Mech.* **2022**, *14*, 2150131. [[CrossRef](#)]
38. Van Vinh, P.; Van Chinh, N.; Tounsi, A. Static bending and buckling analysis of bi-directional functionally graded porous plates using an improved first-order shear deformation theory and FEM. *Eur. J. Mech.-A/Solids* **2022**, *96*, 104743. [[CrossRef](#)]
39. Larbi, L.O.; Kaci, A.; Houari, M.S.A.; Tounsi, A. An efficient shear deformation beam theory based on neutral surface position for bending and free vibration of functionally graded beams. *Mech. Based Des. Struct. Mach.* **2013**, *41*, 421–433. [[CrossRef](#)]
40. Eltaher, M.A.; Abdelrahman, A.A.; Al-Nabawy, A.; Khater, M.; Mansour, A. Vibration of nonlinear graduation of nano-Timoshenko beam considering the neutral axis position. *Appl. Math. Comput.* **2014**, *235*, 512–529. [[CrossRef](#)]

41. Eltahir, M.A.; Alshorbagy, A.E.; Mahmoud, F.F. Determination of neutral axis position and its effect on natural frequencies of functionally graded macro/nanobeams. *Compos. Struct.* **2013**, *99*, 193–201. [[CrossRef](#)]
42. Van Do, T.; Doan, D.H.; Duc, N.D.; Bui, T.Q. Phase-field thermal buckling analysis for cracked functionally graded composite plates considering neutral surface. *Compos. Struct.* **2017**, *182*, 542–548. [[CrossRef](#)]
43. Wang, C.M.; Ke, L.; Chowdhury, A.R.; Yang, J.; Kitipornchai, S.; Fernando, D. Critical examination of midplane and neutral plane formulations for vibration analysis of FGM beams. *Eng. Struct.* **2017**, *130*, 275–281. [[CrossRef](#)]
44. Fernando, D.; Wang, C.M.; Chowdhury, A.R. Vibration of laminated-beams based on reference-plane formulation: Effect of end supports at different heights of the beam. *Eng. Struct.* **2018**, *159*, 245–251. [[CrossRef](#)]
45. Zhang, D.G. Modeling and analysis of FGM rectangular plates based on physical neutral surface and high order shear deformation theory. *Int. J. Mech. Sci.* **2013**, *68*, 92–104. [[CrossRef](#)]
46. Shahverdi, H.; Barati, M.R. Vibration analysis of porous functionally graded nanoplates. *Int. J. Eng. Sci.* **2017**, *120*, 82–99. [[CrossRef](#)]
47. Chu, L.; Dui, G.; Zheng, Y. Thermally induced nonlinear dynamic analysis of temperature-dependent functionally graded flexoelectric nanobeams based on nonlocal simplified strain gradient elasticity theory. *Eur. J. Mech.-A/Solids* **2020**, *82*, 103999. [[CrossRef](#)]
48. Babaei, H.; Eslami, M.R. Nonlinear analysis of thermal-mechanical coupling bending of FGP infinite length cylindrical panels based on PNS and NSGT. *Appl. Math. Model.* **2021**, *91*, 1061–1080. [[CrossRef](#)]
49. Babaei, H.; Kiani, Y.; Eslami, M.R. Large amplitude free vibrations of FGM beams on nonlinear elastic foundation in thermal field based on neutral/mid-plane formulations. *Iranian Journal of Science and Technology. Trans. Mech. Eng.* **2021**, *45*, 611–630. [[CrossRef](#)]
50. Touratier, M. An efficient standard plate theory. *Int. J. Eng. Sci.* **1991**, *29*, 901–916. [[CrossRef](#)]
51. Karama, M.; Afaq, K.S.; Mistou, S. Mechanical behaviour of laminated composite beam by the new multi-layered laminated composite structures model with transverse shear stress continuity. *Int. J. Solids Struct.* **2003**, *40*, 1525–1546. [[CrossRef](#)]
52. Reddy, J. Nonlocal theories for bending, buckling and vibration of beams. *Int. J. Eng. Sci.* **2007**, *45*, 288–307. [[CrossRef](#)]
53. Thai, H.T.; Kim, S.E. Levy-type solution for free vibration analysis of orthotropic plates based on two variable refined plate theory. *Appl. Math. Model.* **2012**, *36*, 3870–3882. [[CrossRef](#)]
54. Taibi, F.Z.; Benyoucef, S.; Tounsi, A.; Bachir Bouiadjra, R.; Adda Bedia, E.A.; Mahmoud, S.R. A simple shear deformation theory for thermo-mechanical behaviour of functionally graded sandwich plates on elastic foundations. *J. Sandw. Struct. Mater.* **2015**, *17*, 99–129. [[CrossRef](#)]
55. Attia, M.A.; Mohamed, S. Thermal vibration characteristics of pre/post-buckled bi-directional functionally graded tapered microbeams based on modified couple stress Reddy beam theory. *Eng. Comput.* **2020**, 1–27. [[CrossRef](#)]
56. Pham, Q.H.; Nguyen, P.C.; Tran, V.K.; Nguyen-Thoi, T. Isogeometric analysis for free vibration of bidirectional functionally graded plates in the fluid medium. *Defence Technol.* **2022**, *18*, 1311–1329. [[CrossRef](#)]
57. Coskun, S.; Kim, J.; Toutanji, H. Bending, free vibration, and buckling analysis of functionally graded porous micro-plates using a general third-order plate theory. *J. Compos. Sci.* **2019**, *3*, 15. [[CrossRef](#)]
58. Zur, K.K.; Arefi, M.; Kim, J.; Reddy, J.N. Free vibration and buckling analyses of magneto-electro-elastic FGM nanoplates based on nonlocal modified higher-order sinusoidal shear deformation theory. *Compos. Part B Eng.* **2020**, *182*, 107601. [[CrossRef](#)]
59. Shu, C. *Differential Quadrature and Its Application in Engineering*; Springer Science & Business Media: Berlin, Germany, 2012.
60. Shanab, R.A.; Attia, M.A.; Mohamed, S.A. Nonlinear analysis of functionally graded nanoscale beams incorporating the surface energy and microstructure effects. *Int. J. Mech. Sci.* **2017**, *131–132*, 908–923. [[CrossRef](#)]
61. Mohamed, S.A. A fractional differential quadrature method for fractional differential equations and fractional eigenvalue problems. *Math. Methods Appl. Sci.* **2020**. [[CrossRef](#)]
62. Mohamed, S.A.; Mohamed, N.A.; Abo-Hashem, S.I. A novel differential-integral quadrature method for the solution of nonlinear integro-differential equations. *Math. Methods Appl. Sci.* **2021**, *44*, 13945–13967. [[CrossRef](#)]
63. Singha, M.K.; Prakash, T.; Ganapathi, M. Finite element analysis of functionally graded plates under transverse load. *Finite Elem. Anal. Des.* **2011**, *47*, 453–460. [[CrossRef](#)]
64. Zenkour, A.M. Generalized shear deformation theory for bending analysis of functionally graded plates. *Appl. Math. Model.* **2006**, *30*, 67–84. [[CrossRef](#)]
65. Mohamed, M.; Abdelouahed, T.; Slimane, M. A refined of trigonometric shear deformation plate theory based on neutral surface position is proposed for static analysis of FGM plate. *Procedia Struct. Integr.* **2020**, *26*, 129–138. [[CrossRef](#)]
66. Thai, H.T.; Choi, D.H. A refined plate theory for functionally graded plates resting on elastic foundation. *Compos. Sci. Technol.* **2011**, *71*, 1850–1858. [[CrossRef](#)]
67. Zenkour, A.M.; Sobhy, M. Dynamic bending response of thermoelastic functionally graded plates resting on elastic foundations. *Aerosp. Sci. Technol.* **2013**, *29*, 7–17. [[CrossRef](#)]
68. Benahmed, A.; Houari, M.S.A.; Benyoucef, S.; Belakhdar, K.; Tounsi, A. A novel quasi-3D hyperbolic shear deformation theory for functionally graded thick rectangular plates on elastic foundation. *Geomech. Eng.* **2017**, *12*, 9–34. [[CrossRef](#)]